

# Dalton Transactions

Accepted Manuscript



This is an *Accepted Manuscript*, which has been through the Royal Society of Chemistry peer review process and has been accepted for publication.

*Accepted Manuscripts* are published online shortly after acceptance, before technical editing, formatting and proof reading. Using this free service, authors can make their results available to the community, in citable form, before we publish the edited article. We will replace this *Accepted Manuscript* with the edited and formatted *Advance Article* as soon as it is available.

You can find more information about *Accepted Manuscripts* in the [Information for Authors](#).

Please note that technical editing may introduce minor changes to the text and/or graphics, which may alter content. The journal's standard [Terms & Conditions](#) and the [Ethical guidelines](#) still apply. In no event shall the Royal Society of Chemistry be held responsible for any errors or omissions in this *Accepted Manuscript* or any consequences arising from the use of any information it contains.



[www.rsc.org/dalton](http://www.rsc.org/dalton)

# Heterodinuclear (Sm, Tb) lanthanide pivalates with heterocyclic N-donors: synthesis, structure, thermal behavior, magnetic and photoluminescence properties

Irina G. Fomina,<sup>\*</sup> Zhanna V. Dobrokhotova, Andrey B. Ilyukhin, Valery I. Zhilov, Artem S. Bogomyakov, Andrey A. Antoshkov, Yury S. Zavorotny, Vasilisa I. Gerasimova, Vladimir M. Novotortsev, and Igor L. Eremenko

*N.S. Kurnakov Institute of General and Inorganic Chemistry, Russian Academy of Sciences, Leninsky Prosp. 31, 119991 Moscow, Russian Federation. E-mail: fomina@igic.ras.ru*

†Electronic supplementary information (ESI) available: CCDC reference numbers 987077 (for **1**), 987035 (for **2a**·1.75EtOH), 1025082 (for **2b**·2EtOH), and 945158 (for **2b**·EtOH). This material is available free of charge from the Cambridge Crystallographic Data Centre via [www.ccdc.cam.ac.uk/data\\_request/cif](http://www.ccdc.cam.ac.uk/data_request/cif). Crystallographic parameters and structure refinement statistics for compounds **1**, **2a**·1.75EtOH, **2b**·2EtOH, and **2b**·EtOH (Table S1). Further synthetic details and analytical data for **2b**·EtOH (Fig. S1). Mass spectra of **1** and **2a**·1.75EtOH (Table S2). Selected bond lengths and Ln...Ln distances in **1**, **2a**·1.75EtOH, **2b**·2EtOH, and **2b**·EtOH (Table S3). PL spectra and scattering spectra of **7** (Fig. S2). PL spectra of **7** and **8** (Fig. S3).

## Abstract

Heterobimetallic complexes [SmTb(piv)<sub>6</sub>(phen)<sub>2</sub>] (**1**), [SmTb(piv)<sub>6</sub>(bath)<sub>2</sub>]·1.75EtOH (**2a**·1.75EtOH), [SmTb(piv)<sub>6</sub>(bath)<sub>2</sub>]·2EtOH (**2b**·2EtOH), and [SmTb(piv)<sub>6</sub>(bath)<sub>2</sub>]·EtOH (**2b**·EtOH) where piv is (CH<sub>3</sub>)<sub>3</sub>CCO<sub>2</sub><sup>-</sup>, phen is 1,10-phenanthroline, and bath is 4,7-diphenyl-1,10-phenanthroline, were synthesized and studied by X-ray diffraction. It was shown, that complexes **2a**·1.75EtOH and **2b**·2EtOH have different molecular and crystal structures. Complexes **2a**·1.75EtOH, **2b**·2EtOH, and **2b**·EtOH differ by the structural functions of μ<sub>2</sub>-piv anions. **2a**·1.75EtOH contains two μ<sub>2</sub>-piv-κ<sup>2</sup>O,O' anions and two μ<sub>2</sub>-piv-κ<sup>2</sup>O,O,O' anions, whereas **2b**·2EtOH and **2b**·EtOH have four μ<sub>2</sub>-piv-κ<sup>2</sup>O,O' anions. According to the mass spectrometry data, the dimeric molecules [SmTb(piv)<sub>6</sub>] is the the major part metal-containing component of gas-phase complexes **1**, **2a**·1.75EtOH, and **2b**·2EtOH. The characteristic features of the thermal behavior of these complexes were revealed, and their magnetic and photoluminescence (PL) properties were

investigated. A unique feature of desolvated complexes **2a**·1.75EtOH and **2b**·2EtOH is melting at high temperatures before thermal decomposition. Magnetic properties of **1** and **2a**·1.75EtOH are determined mainly by the Tb<sup>3+</sup> ions. The optical properties of these complexes and their homodinuclear analogs were analyzed by photoluminescence, excitation, phosphorescence, and scattering spectroscopy and by lifetime measurements at 77 K and 300 K. As the temperature decreases to 77 K, the PL intensity of Tb<sup>3+</sup> ions in **1** and **2a**·1.75EtOH substantially increases by 40 and 100 times, respectively, compared to 300 K. The PL color evidently changes from red at 300 K to bright green at 77 K. Based on these results, the mechanism of intramolecular energy transfer between the ligand levels and Sm<sup>3+</sup> and Tb<sup>3+</sup> ions under UV radiation was proposed.

## Introduction

Metal-organic coordination compounds of lanthanides have unique physicochemical properties and hold promise for the design of novel molecular materials with various functional characteristics, such as magnetic, optical, sorption, catalytic, and so on.<sup>1</sup> This is why researchers are paying increasing attention not only to the development of new approaches and methods for the synthesis of this class of compounds but also to detailed investigation of their chemical and physical properties.<sup>2</sup> Lanthanide-containing complexes, which have, as a rule, unpaired *f* electrons (except for La(III)) and include organic components (bridging and terminal ligands), serve as carriers of “properties” of magnetically and optically active materials based on these compounds. In most cases, such molecular systems are polyfunctional since they not only have unusual magnetic properties but often also exhibit luminescence properties, thus substantially increasing the functional potential of these substances. The advantages of lanthanide luminescence are characteristic narrow line-like emission bands mostly in the visible and near-IR spectral regions, long lifetimes (from μs to ms), and high quantum yields. Due to low extinction coefficients of the Laporte-forbidden *f*-*f* transitions, lanthanide(III) ions are indirectly excited by organic ligands or “antennas” that possess a reasonably large molar absorption cross section<sup>3</sup> followed by efficient energy transfer to metal ion excited states. Then the excitation energy is emitted as a characteristic Ln(III) emission line due to *f*-*f* transitions. It should be noted that for heterobimetallic compounds, it is necessary to take into account not only the antenna effect but also the possibility of the complete or partial excitation energy transfer from 4*f* levels of one metal to 4*f* levels of another one.<sup>4</sup> This gives rise to competitive excited state relaxation pathways in the molecular system, which offers prospects for

the design of controlled luminescence sensors. It is evident that the synthesis of novel dinuclear molecules of this type containing different lanthanide atoms in the metal core will substantially increase the range of varying new properties of molecular materials.

Recently,<sup>4h</sup> we have reported methods for the synthesis, structures, and thermal decomposition of magnetic luminescent heterobimetallic pivalate (trimethylacetate, piv<sup>-</sup> is (CH<sub>3</sub>)<sub>3</sub>CCO<sub>2</sub><sup>-</sup>) complexes of Eu(III) and Tb(III) with coordinated pivalic acid (Hpiv) or 1,10-phenanthroline (phen) molecules. It was shown that in these complexes, the <sup>5</sup>D<sub>3</sub>(Tb<sup>3+</sup>) → 4f(Eu<sup>3+</sup>) excitation energy transfer can take place. In the present work, we studied the photophysical properties and examined the possibility of such excitation energy transfer in the synthesized heterobimetallic dinuclear pivalates containing Sm(III) and Tb(III) atoms in 1 : 1 ratio and chelating N-donor phen or 4,7-diphenyl-1,10-phenanthroline (bath) ligands. The new complexes were studied by X-ray diffraction and gas-phase mass spectrometry. Their thermal behavior was investigated by differential scanning calorimetry (DSC) and thermogravimetric analysis (TGA), and their magnetic properties were studied as well.

## Experimental

### Synthesis

The starting complexes [Sm<sub>2</sub>(piv)<sub>6</sub>(Hpiv)<sub>6</sub>]·Hpiv and [Tb<sub>2</sub>(piv)<sub>6</sub>(Hpiv)<sub>6</sub>] and known compounds [Tb<sub>2</sub>(piv)<sub>6</sub>(phen)<sub>2</sub>] (**3**), [Sm<sub>2</sub>(piv)<sub>6</sub>(phen)<sub>2</sub>] (**4**), [Sm<sub>2</sub>(piv)<sub>6</sub>(bath)<sub>2</sub>]·2EtOH (**5a**·2EtOH), and [Tb<sub>2</sub>(piv)<sub>6</sub>(bath)<sub>2</sub>]·1.5EtOH (**6a**·1.5EtOH) were prepared according to previously reported procedures.<sup>5</sup> The synthesis was carried out using standard Schlenk techniques. Analytical-grade reagents and solvents were commercially available. Pivalic acid, Hpiv (Acros Organics); Sm(OAc)<sub>3</sub>·xH<sub>2</sub>O, Tb(OAc)<sub>3</sub>·xH<sub>2</sub>O, and phen·H<sub>2</sub>O (Alfa Aesar); bath and EtOH (Aldrich) were used without further purification. The water content in Sm(OAc)<sub>3</sub>·xH<sub>2</sub>O and Tb(OAc)<sub>3</sub>·xH<sub>2</sub>O was determined by thermogravimetric analysis.

**Synthesis of [SmTb(piv)<sub>6</sub>(phen)<sub>2</sub>] (**1**).** To [Sm<sub>2</sub>(piv)<sub>6</sub>(Hpiv)<sub>6</sub>]·Hpiv (0.25 g, 0.15 mmol), [Tb<sub>2</sub>(piv)<sub>6</sub>(Hpiv)<sub>6</sub>] (0.25 g, 0.15 mmol), and Phen·H<sub>2</sub>O (0.39 g, 1.96 mmol), ethanol (50 ml) was added. The reaction mixture was heated in air at 80 °C until the starting reagents completely dissolved. The solution was filtered, concentrated at 0.1 Torr and 20 °C to 30 mL, and kept at 20 °C. Crystals of **1** that precipitated within 24 h were separated by decantation, washed with cold ethanol,

and dried in air. The crystals that formed in the course of the synthesis were used for X-ray diffraction. The single phase of **1** was confirmed by X-ray powder diffraction. The yield of compound **1** was 0.38 g (92%, with respect to the starting terbium compound). The evaluated stoichiometry of Sm and Tb atoms in the crystal of **1** is  $1.03\pm 0.05 : 1.02\pm 0.05$ . Found (%): C, 50.89; H, 5.71; N, 4.53.  $C_{54}H_{70}Sm_{1.0}N_4O_{12}Tb_{1.0}$ . Calculated (%): , 50.81; H, 5.53; N, 4.39. FT-IR (KBr),  $\nu/cm^{-1}$ : 3056 m, 2976 s, 2954 s, 2924 s, 2902 s, 2866 s, 1624 w, 1579 m, 1536 m, 1516 s, 1483 s, 1456 s, 1426 s, 1371 s, 1360 s, 1302 w, 1227 s, 1143 m, 1103 m, 1044 w, 1028 m, 980 s, 937 w, 904 w, 893 s, 863 s, 852 s, 833 w, 806 s, 794 s, 731 s, 721 m, 669 w, 635 w, 603 m, 586 m, 556 m, 544 m, 474 w, 463 w, 418 m.

**Synthesis of [SmTb(piv)<sub>6</sub>(bath)<sub>2</sub>] $\cdot$ 1.75EtOH (2a $\cdot$ 1.75EtOH).** To [Sm<sub>2</sub>(piv)<sub>6</sub>(Hpiv)<sub>6</sub>] $\cdot$ Hpiv (0.51 g, 0.33 mmol), [Tb<sub>2</sub>(piv)<sub>6</sub>(Hpiv)<sub>6</sub>] (0.54 g, 0.33 mmol), and bath (1.3 g, 3.91 mmol), ethanol (50 ml) was added. The reaction mixture was heated in air at 80 °C until the starting reagents completely dissolved. The solution was filtered and kept at 5 °C for 24 h. Colorless prismatic crystals of the compound suitable for X-ray study that precipitated were separated by decantation, washed with cold ethanol, and dried in air. The single phase of **2a** $\cdot$ 1.75EtOH was confirmed by X-ray powder diffraction. The yield of compound **2a** $\cdot$ 1.75EtOH was 0.63 g (0.38 mmol, 54% with respect to the starting terbium compound). The evaluated stoichiometry of Sm and Tb atoms in the crystal of **2a** $\cdot$ 1.75EtOH is  $1.02\pm 0.05 : 1.04\pm 0.05$ . Found (%): C, 59.06; H, 6.11; N, 3.59.  $C_{81.50}H_{96.5}Sm_{1.0}N_4O_{13.75}Tb_{1.0}$ . Calculated (%): C, 58.92; H, 5.85; N, 3.37. FT-IR (KBr),  $\nu/cm^{-1}$ : 3410 m, 3061 m, 2980 s, 2954 s, 2925 m, 2866 m, 1620 s, 1589 s, 1580 s, 1559 s, 1533 s, 1522 m, 1494 m, 1482 s, 1459 m, 1446 m, 1421 s, 1372 w, 1379 s, 1360 s, 1285 m, 1226 s, 1155 w, 1112 w, 1092 m, 1080 w, 1046 w, 1028 w, 1001 w, 973 w, 934 w, 890 m, 877 w, 855 m, 832 m, 804 m, 795 m, 771 m, 766 m, 741 m, 704 m, 666 w, 627 m, 602 s, 595 m, 575 m, 564 m, 544 m, 487 w, 464 w.

**Synthesis of [SmTb(piv)<sub>6</sub>(bath)<sub>2</sub>] $\cdot$ 2EtOH (2b $\cdot$ 2EtOH).** Needle-like colorless crystals of **2b** $\cdot$ 2EtOH that formed within 36 h from the solution, which remained after the decantation of **2a** $\cdot$ 1.75EtOH, were separated by decantation, washed with cold ethanol, and dried in air. The crystals of the compound obtained in the synthesis were suitable for X-ray diffraction. The single phase of **2b** $\cdot$ 2EtOH was confirmed by X-ray powder diffraction. The yield of compound **2b** $\cdot$ 2EtOH was 0.25 g (0.15 mmol, 21% with respect to the starting terbium compound). The evaluated stoichiometry of Sm and Tb atoms in the crystal of **2b** $\cdot$ 2EtOH is  $1.02\pm 0.05 : 1.03\pm 0.05$ . Found (%):

C, 58.99; H, 6.03; N, 3.41.  $C_{82}H_{98}Sm_{1.0}N_4O_{14}Tb_{1.0}$ . Calculated (%): C, 58.87; H, 5.90; N, 3.35. FT-IR (KBr),  $\nu/cm^{-1}$ : 3424 m, 3082 w, 3060 m, 3033 w, 2959 s, 2924 m, 2902 m, 2865 m, 1623 s, 1594 s, 1580 m, 1564 s, 1532 s, 1521 s, 1483 s, 1458 m, 1445 m, 1423 s, 1389 m, 1376 s, 1360 s, 1287 m, 1227 s, 1159 w, 1111 w, 1092 m, 1074 w, 1028 w, 1020 w, 1000 w, 988 w, 976 w, 937 w, 893 m, 878 w, 868 w, 856 m, 833 m, 807 m, 795 m, 789 m, 765 m, 743 m, 703 s, 665 w, 629 m, 607 m, 595 s, 575 m, 564 m, 549 m, 497 w, 488 w, 476 w, 434 w.

**Synthesis of  $[SmTb(piv)_6(bath)_2]\cdot EtOH$  (**2b** $\cdot EtOH$ )** was prepared by the desolvation of **2b** $\cdot 2EtOH$  in the presence of  $CaCl_2$ . Further details of the synthesis and analytical data for **2b** $\cdot EtOH$  are given in Fig. S1†.

## Methods

The elemental analyses were carried out on an Euro Vector Element Analyser CHN elemental analyzer (Model EA 3000). The stoichiometry of samarium and terbium in **1**, **2a** $\cdot 1.75EtOH$ , **2b** $\cdot 2EtOH$ , and **2b** $\cdot EtOH$  was determined by inductively coupled plasma atomic emission spectrometry (ICP-AES) on an IRIS Advantage spectrometer. The IR spectra were measured using a Perkin Elmer Spectrum-65LS FT-IR spectrometer ( $400\text{--}4000\text{ cm}^{-1}$ ). The magnetic susceptibility of the polycrystalline samples was measured with a Quantum Design MPMSXL SQUID magnetometer in the temperature range 2-300 K with magnetic field of up to 5 kOe.

## X-ray data collection

X-ray diffraction data were collected on a Bruker SMART APEX2 diffractometer<sup>6</sup> at the Center of Collaborative Research of IGIC RAS (Table S1†). The semi-empirical absorption correction from equivalents was applied using the SADABS program.<sup>7</sup> The atomic coordinates of isostructural compounds<sup>4h,5b,5c,5d</sup> were used as the starting models. The X-ray diffraction data sets for **2b** $\cdot 2EtOH$  at 173 K and for **2b** $\cdot EtOH$  at 296 K were collected from different single crystals. In the calculations, the Sm : Tb ratio in **1**, **2a** $\cdot 1.75EtOH$ , **2b** $\cdot 2EtOH$ , and **2b** $\cdot EtOH$  was taken equal to 1 : 1. In the refinement, geometric restraints were placed on the disordered *tert*-Bu groups of piv ligands. In structure **2b** $\cdot EtOH$  the highest difference peak ( $1.46\text{ e}/\text{\AA}^3$ ) is located at distances of 2.04 and 2.32 Å from both positions of a carbon atom of a disordered *tert*-Bu group of a piv ligand. All calculations were carried out using the SHELXL-2013 software.<sup>8</sup>

## Mass spectrometry

The electron impact ionization mass spectra were obtained on an Incos 50 mass spectrometer (Finnigan, USA) at 70 eV electron energy. The calibration was performed in the  $m/z$  range of 169 – 1000 using Fomblin Y HVAC 25/9 and reference ions at  $m/z$  169, 335, 501, 667, 783, 849, 999;<sup>9</sup> the temperature of the ion source was 250 °C. The spectra were obtained by scanning in the  $m/z$  range from 170 to 1000; the scan rate was 1 scan/s. A solution or a suspension of the sample in  $\text{CH}_2\text{Cl}_2$  was injected into an ampoule of the inlet system for introducing solid and liquid samples, and the sample was vaporized at room temperature under reduced pressure in a vacuum desiccator containing molecular sieves and paraffin. Samples were injected into the ion source using the direct insertion probe (DIP). The initial temperature was 50 °C, and the heating rate was 15 °C/min to 350 °C. The mass spectra of complexes  $[\text{SmTb}(\text{piv})_6(\text{phen})_2]$  (**1**) and  $[\text{SmTb}(\text{piv})_6(\text{bath})_2] \cdot 1.75\text{EtOH}$  (**2a**·1.75EtOH) are given in Table S2†.

## Thermal behavior

The thermal behavior was studied by differential scanning calorimetry (DSC) and thermogravimetric analysis (TGA). Thermogravimetric analysis was performed under an argon flow (Ar, > 99.998 %;  $\text{O}_2$ , < 0.0002 %;  $\text{N}_2$ , < 0.001 %; water vapor, < 0.0003 %;  $\text{CH}_4$ , < 0.0001 %) (20 mL/min) on a *NETZSCH TG 209 F1* instrument at a heating rate of 10 °C/min. The gas-phase composition at temperatures below 300 °C was studied by thermogravimetry-mass spectrometry on a QMS 403C Aëolos quadrupole mass spectrometer. The ionizing electron energy was 70 eV; the largest measured mass number (the ratio of the mass of the ion to its charge  $Z$ ) was 300 amu. Differential scanning calorimetry studies were carried out under an argon flow on a *NETZSCH DSC 204 F1* calorimeter at a heating rate of 5 °C/min. The weights of the samples were 4–10 mg. Each experiment was repeated at least three times. The temperature calibration of the thermobalance was made based on the phase transition points of reference compounds. The calorimeter was calibrated with the ISO 11357-1 standard for the temperature and heat flow. The thermal analysis data were analyzed according to ISO 11357-1, ISO 11357-2, ISO 11358, and ASTM E 1269-95 standards using the *NETZSCH Proteus Thermal Analysis* software package. The X-ray powder diffraction analysis of the decomposition products was carried out with a FR-552 Guinier camera ( $\text{CuK}_{\alpha 1}$

radiation, monochromator) using germanium as the internal standard (the X-ray diffraction patterns were processed with an IZA-2 comparator with an accuracy of  $\pm 0.01$  mm) and the STOE Powder Diffraction System.

### Photoluminescence spectrometry

Photoluminescence (PL) spectra were recorded on a USB4000 spectrometer (Ocean Optics) at 77 and 300 K using an AIL-3 nitrogen laser (excitation wavelength  $\lambda_{\text{ex}} = 337$  nm, average power 3.6 mW) as the PL excitation source. Polycrystalline samples were ground and mixed with a neutral immersion liquid (silicone oil) in a ratio of 3 mg of the sample per microliter of the oil. The mixture was placed between thin quartz glass plates separated by a 40  $\mu\text{m}$  thick aluminum foil tape. PL was excited at an angle of  $80^\circ$  to the plate surface, and PL was measured at an angle of  $55^\circ$  to the incident beam. A quartz lens with a focal distance of 10 mm was used to form an image at the spectrometer slit. Due to the same spectrometer configuration for all the samples under study and the fact that the level of laser radiation absorption at a depth of all samples was 100%, it was possible to directly compare the PL line intensities in the spectra of the compounds. All spectra were corrected for the spectral sensitivity of the spectrometer. The scattering spectra were recorded in the range of 200-450 nm at 300 K using a MDR-6 monochromator (spectral resolution 0.78 nm) and a FEU-100 photoelectron multiplier; a DDS-30 deuterium lamp was used as an excitation source for PL. The scattering spectrum of MgO obtained under the same conditions was used as the correction spectrum. The excitation spectra were recorded in the range of 300-500 nm at 300 K using a MDR-6 monochromator (spectral resolution 1.56 nm) and a FEU-100 photoelectron multiplier in the detection channel and using a MDR-12 monochromator (spectral resolution 2.4 nm) and a xenon lamp (35 W) in the excitation channel. The spectra were corrected for the spectral brightness in the excitation channel. To study the PL decay kinetics, an AIL-3 nitrogen laser was used as the pulse excitation source. The detection system consisted of an R-300 photoelectron multiplier (Hamamatsu), a preamplifier with the integration constant of no longer than 17  $\mu\text{s}$ , a MUM miniature monochromator (spectral resolution 1 nm), and a BS-8 color light filter. The PL decay kinetics was measured using a Tektronix TDS1012 digital storage oscilloscope.

Table 1 gives the relative integrated quantum yields  $K_{\text{rel}}$  for all samples based on the PL spectra and the measured level of absorption at an excitation wavelength ( $\lambda_{\text{ex}} = 337$  nm). The absolute

quantum yield  $K$  is the ratio of the number of quanta absorbed ( $N_{abs}$ ) to the number of quanta emitted ( $N_{emit}$ );  $N_{abs}$  and  $N_{emit}$  can be given by the formulas (1) and (2), respectively.

$$N_{abs} = P_{aver} \cdot \exp^{-\alpha L} \cdot \left(\frac{hc}{\lambda}\right)^{-1}, \quad (1)$$

where  $N_{abs}$  [ $s^{-1}$ ] is the number of quanta absorbed per second,  $P_{aver} = 3.6$  mW is the average power of the pump source,  $\alpha$  [ $cm^{-1}$ ] is the absorption coefficient at the pump wavelength,  $L$  [cm] is the thickness of the sample, and  $\frac{hc}{\lambda} = 5.9 \cdot 10^{-16}$  mJ is the energy of the quantum at the pump wavelength  $\lambda_{ex} = 337$  nm.

$$N_{emit} = C \cdot \int_{\nu_{min}}^{\nu_{max}} I(\nu) d\nu, \quad (2)$$

where  $N_{emit}$  [ $s^{-1}$ ] is the number of quanta emitted per second,  $I$  [ $W\ cm^{-1}$ ] is the spectral density of radiation,  $\nu_{min}$  and  $\nu_{max}$  [ $cm^{-1}$ ] are the limits of the measured spectral range,  $C$  [ $cm\ J^{-1}$ ] is the coefficient determined by the geometry of the experiment (the sizes and shapes of the samples, the relative slit of the spectrometer, and so on). Since it is impossible to precisely measure or estimate the value of  $C$  but, nevertheless, it was one and the same for all the samples and measurements because the samples have the same shape (see above), which was the condition of our experiments, we give the relative quantum yields  $K_{rel}(i)$ :

$$K_{rel}(i) = \frac{K(i)}{K(3)}, \quad (3)$$

where  $K(3)$  is the quantum yield in complex  $[Tb_2(piv)_6(phen)_2]$  (3).

To compare the efficiency of the emission channels for the relaxation of the excitation energy in every homo- and heterobimetallic complex, we used the parameter  $\xi$ , which indicates the percentage of quanta per a particular emission channel for energy relaxation ( $Tb^{3+}$ ,  $Sm^{3+}$ , or the N-donor ligand (L)) in the total ensemble  $N_{emit}$ . To determine  $\xi$ , the measured PL spectral range was divided into two or three segments, the limits of which were specified for each particular sample. Their numerical values are given in parentheses in Table 1. It should be noted that for each complex, the product  $K_{rel}(i) \cdot \xi$  characterizes the relative quantum yield of PL of a particular  $Ln^{3+}$  or L in the complex under consideration.

**Table 1.** Numerical parameters of PL for complexes **1**, **2a**·1.75EtOH, **3**, **4**, **5a**·2EtOH, and **6a**·1.5EtOH:  $K_{rel}$  is the relative integrated quantum yield of PL,  $\xi$  is the relative quantum efficiency

of emission channels for energy relaxation. The integration limits  $\lambda_{\min}$  and  $\lambda_{\max}$  [nm] are given in square brackets.

Complex	$K_{rel}$ [360;740]	$\xi$ , %		
		L	Tb <sup>3+</sup>	Sm <sup>3+</sup>
<b>1</b>	0.0097	2 [360;480]	12 [480;555]	86 [555;740]
<b>2a</b> ·1.75EtOH	0.0077	4 [360;480]	6 [480;555]	90 [555;740]
<b>3</b>	<b>1.0000</b>	<0.01 [360;480]	>99.99 [480;740]	-
<b>4</b>	0.0007	43 [360;540]	-	57 [540;740]
<b>5a</b> ·2EtOH	0.0018	73 [360;540]	-	27 [540;740]
<b>6a</b> ·1.5EtOH	0.0019	12 [360;480]	88 [480;740]	-

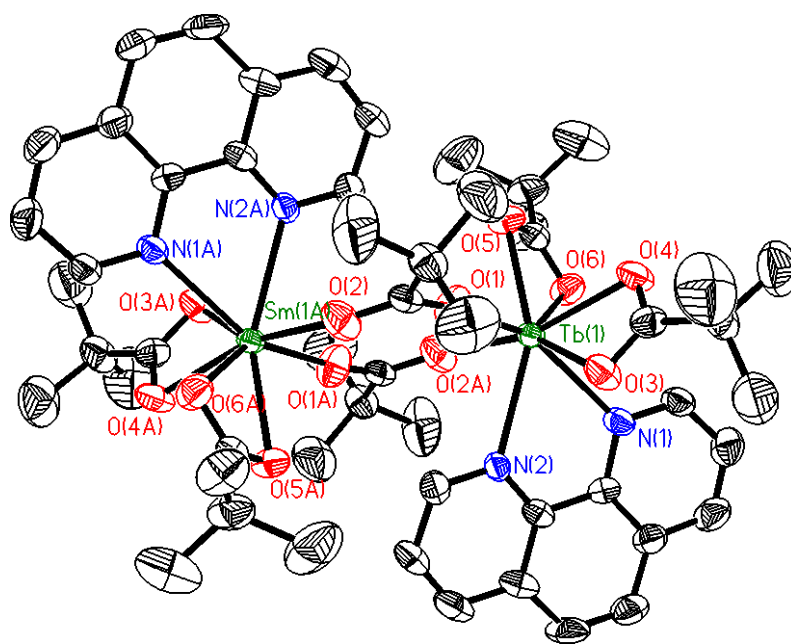
## Results and discussion

### Synthesis and X-ray diffraction analysis

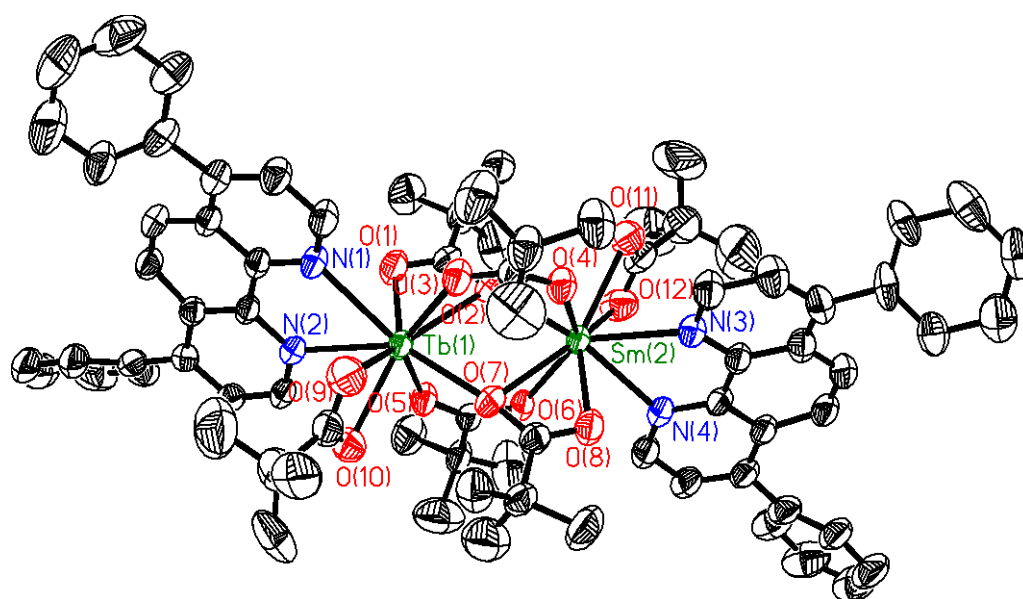
Earlier, we have shown that pivalates  $[\text{Ln}_2(\text{piv})_6(\text{Hpiv})_6]$  ( $\text{Ln}_2 = \text{Sm}_2, \text{Eu}_2, \text{Gd}_2, \text{Tb}_2, \text{EuTb}$ ) readily react with an excess of heterocyclic N-donor ligands in EtOH under reflux to form the dinuclear complexes  $[\text{Ln}_2(\text{piv})_6\text{L}_2]$ , where L = bpy or phen, and  $[\text{Ln}_2(\text{piv})_6(\text{bath})_2] \cdot x\text{Solv}$ , where  $x = 0-2$  and Solv = EtOH or H<sub>2</sub>O.<sup>4h,5,10</sup> The heterobimetallic pivalates  $[\text{SmTb}(\text{piv})_6(\text{phen})_2]$  (**1**),  $[\text{SmTb}(\text{piv})_6(\text{bath})_2] \cdot 1.75\text{EtOH}$  (**2a**·1.75EtOH) and  $[\text{SmTb}(\text{piv})_6(\text{bath})_2] \cdot 2\text{EtOH}$  (**2b**·2EtOH) were obtained in the form of single crystals suitable for X-ray diffraction by the same method using  $[\text{Sm}_2(\text{piv})_6(\text{Hpiv})_6] \cdot \text{Hpiv}$  and  $[\text{Tb}_2(\text{piv})_6(\text{Hpiv})_6]$  in a molar ratio of 1 : 1 as the starting metal-containing reagents. Complex  $[\text{SmTb}(\text{piv})_6(\text{bath})_2] \cdot \text{EtOH}$  (**2b**·EtOH) was prepared by the desolvation of **2b**·2EtOH in the presence of CaCl<sub>2</sub>. According to the ICP-AES data, the ratio of Sm to Tb atoms in the crystals of **1**, **2a**·1.75EtOH, **2b**·2EtOH, and **2b**·EtOH is 1.03(5) : 1.02(5), 1.02(5) : 1.04(5), 1.02(5) : 1.03(5), and 1.02(5) : 1.03(5), respectively.

According to the X-ray diffraction data, complexes  $[\text{SmTb}(\text{piv})_6(\text{phen})_2]$  (**1**),  $[\text{SmTb}(\text{piv})_6(\text{bath})_2] \cdot 1.75\text{EtOH}$  (**2a**·1.75EtOH),  $[\text{SmTb}(\text{piv})_6(\text{bath})_2] \cdot 2\text{EtOH}$  (**2b**·2EtOH), and  $[\text{SmTb}(\text{piv})_6(\text{bath})_2] \cdot \text{EtOH}$  (**2b**·EtOH) have a dinuclear structure typical of Ln carboxylates (Fig. 1, Table S3†). Complex **1** (Fig. 1a) is isostructural with the known pivalates  $[\text{Tb}_2(\text{piv})_6(\text{phen})_2]$  (**3**),<sup>5b</sup>  $[\text{EuTb}(\text{piv})_6(\text{phen})_2]$ .<sup>4h</sup> The coordination number of the metal atom in **1** is 8 due to coordination of

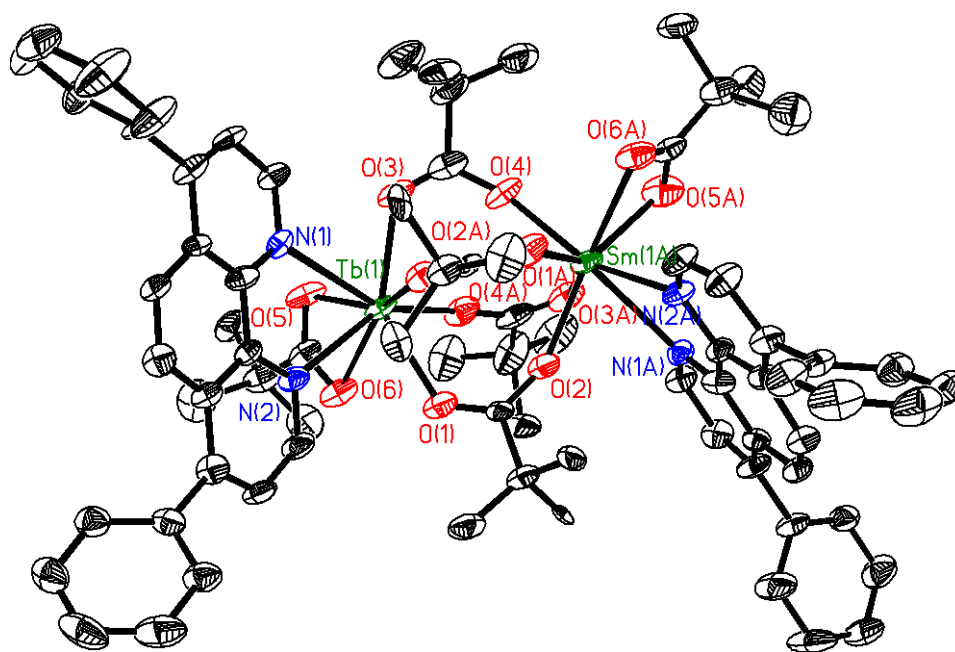
the metal atom by six oxygen atoms of two  $\mu_2$ -piv- $\kappa^2$ O,O' anions and two piv- $\kappa^2$ O,O' anions and two nitrogen atoms of phen- $\kappa^2$ N,N'. The structure of complex **1** differs from those of phenanthroline pivalates of similar composition [Sm<sub>2</sub>(piv)<sub>6</sub>(phen)<sub>2</sub>] (**4**),<sup>5c</sup> [Eu<sub>2</sub>(piv)<sub>6</sub>(phen)<sub>2</sub>],<sup>5b</sup> and [Gd<sub>2</sub>(piv)<sub>6</sub>(phen)<sub>2</sub>],<sup>5b</sup> in which the metal atoms have coordination number 9 as a result of the binding to seven oxygen atoms of two  $\mu_2$ -piv- $\kappa^2$ O,O', two  $\mu_2$ -piv- $\kappa^2$ O,O,O', and two piv- $\kappa^2$ O,O' anions and two nitrogen atoms of phen- $\kappa^2$ N,N'. Complexes **2a**·1.75EtOH, **2b**·2EtOH, and **2b**·EtOH differ by the structural functions of the  $\mu_2$ -piv anions. Thus, **2a**·1.75EtOH contains two  $\mu_2$ -piv- $\kappa^2$ O,O' anions and two  $\mu_2$ -piv- $\kappa^2$ O,O,O' anions (Fig. 1b), whereas **2b**·2EtOH and **2b**·EtOH have four  $\mu_2$ -piv- $\kappa^2$ O,O' anions (Fig. 1c). Therefore, the metal atoms in complexes **2a**·1.75EtOH, **2b**·2EtOH, and **2b**·EtOH have different coordination numbers (9 in **2a**·1.75EtOH; 8 in **2b**·2EtOH and **2b**·EtOH). The Ln... Ln' distance in pivalates **1**, **2a**·1.75EtOH, **2b**·2EtOH, and **2b**·EtOH is 5.391(1), 3.9909(4), 4.294(1), and 4.2844(3) Å, respectively. Complex [SmTb(piv)<sub>6</sub>(bath)<sub>2</sub>]·1.75EtOH (**2a**·1.75EtOH) is isostructural with known [Sm<sub>2</sub>(piv)<sub>6</sub>(bath)<sub>2</sub>]·2EtOH (**5a**·2EtOH),<sup>5d</sup> and [Eu<sub>2</sub>(piv)<sub>6</sub>(bath)<sub>2</sub>]·2EtOH,<sup>5b</sup> complex [SmTb(piv)<sub>6</sub>(bath)<sub>2</sub>]·2EtOH (**2b**·2EtOH) is isostructural with known [Sm<sub>2</sub>(piv)<sub>6</sub>(bath)<sub>2</sub>]·2EtOH (**5b**·2EtOH),<sup>5d</sup> [Tb<sub>2</sub>(piv)<sub>6</sub>(bath)<sub>2</sub>] (**6b**) pivalates,<sup>10</sup> respectively. It should be noted that the structure of complexes [SmTb(piv)<sub>6</sub>(bath)<sub>2</sub>]·1.75EtOH (**2a**·1.75EtOH), [Sm<sub>2</sub>(piv)<sub>6</sub>(bath)<sub>2</sub>]·2EtOH (**5a**·2EtOH),<sup>5d</sup> and [Eu<sub>2</sub>(piv)<sub>6</sub>(bath)<sub>2</sub>]·2EtOH<sup>5b</sup> differs from the structure of pivalate [Tb<sub>2</sub>(piv)<sub>6</sub>(bath)<sub>2</sub>]·1.5EtOH (**6a**·1.5EtOH),<sup>5b</sup> which contains only  $\mu_2$ -piv- $\kappa^2$ O,O' anions.



a)



b)



c)

**Fig. 1.** Structures of the complexes in **1** (a), **2a** (b), and **2b** (c). The hydrogen atoms are omitted, only one position of the disordered *tert*-Bu is shown, the Sm and Tb sites are arbitrarily separated.

Recently, it was shown that two different forms of dimeric molecules can exist, as was observed in co-crystals of Tb carboxylates,  $[\text{Tb}_2(\mu_2\text{-iba-}\kappa^2\text{O},\text{O}')_2(\mu_2\text{-iba-}\kappa^2\text{O},\text{O},\text{O}')_2(\text{iba-}\kappa^2\text{O},\text{O}')_2(\text{bpy-}$

$\kappa^2\text{N,N}')$ ][ $\text{Tb}_2(\mu_2\text{-iba-}\kappa^2\text{O,O}')_4(\text{iba-}\kappa^2\text{O,O}')_2(\text{bpy-}\kappa^2\text{N,N}')_2]\cdot 2\text{EtOH}^{11}$  and [ $\text{Tb}_2(\mu_2\text{-mba-}\kappa^2\text{O,O}')_2(\text{mba-}\kappa^2\text{O,O}')_4(\text{phen-}\kappa^2\text{N,N}')_2$ ][ $\text{Tb}_2(\mu_2\text{-mba-}\kappa^2\text{O,O}')_4(\text{mba-}\kappa^2\text{O,O}')_2(\text{phen-}\kappa^2\text{N,N}')_2$ ]<sup>12</sup> (iba is 2-iodobenzoate, mba is 4-methylbenzoate). This supports our statement that the conditions of the synthesis and crystallization, as well as the coordination capacity of lanthanide atoms, have an effect on the molecular and crystal structures of the resulting compounds.

### Thermal behavior

The thermal behavior of complexes [ $\text{Tb}_2(\text{piv})_6(\text{phen})_2$ ] (**3**) and [ $\text{Sm}_2(\text{piv})_6(\text{phen})_2$ ] (**4**) has been studied earlier.<sup>5b,5c</sup> Upon heating under inert atmosphere, heterobimetallic pivalate [ $\text{SmTb}(\text{piv})_6(\text{phen})_2$ ] (**1**) undergoes step-by-step decomposition, as was observed for **3** and **4**. In the thermogravimetric experiments, the weight loss begins at  $257\pm 2$  °C. In the temperature range of 257-340 °C, the mass spectrum shows fragment ions due to the ionization of phen.<sup>13</sup> The characteristics of the thermal decomposition of **1**, **3**, and **4** are given in Table 2. Based on the experimental results, it can be stated that the first step of the thermal decomposition of heterobimetallic pivalate **1**, like that of **3** and **4**, involves the elimination and removal of chelating phen molecules to form the intermediate, *tris*-pivalate [ $\text{Sm}_x\text{Tb}_{1-x}(\text{piv})_3$ ]<sub>n</sub>. The process culminates in the decomposition of the *tris*-pivalate, whereas the formation of the solid decomposition product is apparently completed at temperatures higher than 600 °C. The DSC curves of the first step for complexes [ $\text{SmTb}(\text{piv})_6(\text{phen})_2$ ] (**1**), [ $\text{Tb}_2(\text{piv})_6(\text{phen})_2$ ] (**3**), and [ $\text{Sm}_2(\text{piv})_6(\text{phen})_2$ ] (**4**) were compared (Fig. 2). The difference in their character is clearly visible, which is apparently due to the difference in the structure of the metal carboxylate core of the complexes and, as a consequence, different energy changes after the removal of the neutral phen ligand and the formation of *tris*-pivalates. Presumably, the changes in the coordination sphere of the metal atom after the formation of *tris*-pivalate **4** are associated with the change in the coordination mode of the  $\text{piv-}\kappa^2\text{O,O}'$  and  $\mu_2\text{-piv-}\kappa^2\text{O,O,O}'$  anions. The metal-oxygen bond cleavage is the major process, as evidenced by the presence of one endothermic peak. For **1** and **3**, a complex endothermic peak was observed (the overlap of endothermic and exothermic peaks). This is also indicative of a change in the coordination mode of the piv anions. However, the formation of new bonds in the coordination sphere of the metal atom in the intermediate for these complexes is more essential. This fact suggests that heterobimetallic pivalate **1** is not a mechanical mixture or a solid solution of **3** and **4** but is an individual molecular compound. This approach was proposed for the first time to determine the individuality of heterobimetallic compounds in our earlier study.<sup>4h</sup> It should be noted

that studies of the thermal behavior of carboxylate metal complexes are focused mainly on the determination of their thermal stability, whereas studies of this class of compounds by DSC and TGA in a wide temperature range are scarce.<sup>14</sup> For known carboxylate metal complexes, which have been studied by thermal analytical methods,<sup>15</sup> the fact of structural phase transitions, except for a few examples,<sup>16</sup> and/or the melting before the thermal decomposition was not established.

Investigation of the solid-phase thermal decomposition of heterobimetallic pivalates [SmTb(piv)<sub>6</sub>(bath)<sub>2</sub>] $\cdot$ 1.75EtOH (**2a** $\cdot$ 1.75EtOH) and [SmTb(piv)<sub>6</sub>(bath)<sub>2</sub>] $\cdot$ 2EtOH (**2b** $\cdot$ 2EtOH) showed that these complexes undergo step-by-step decomposition. The first stage corresponds to the removal of solvating molecules (Table 3). At high temperatures, at which no thermal decomposition of complexes as yet occurs, the melting of **2a** $\cdot$ 1.75EtOH and **2b** $\cdot$ 2EtOH takes place, as in the case of samarium complexes [Sm<sub>2</sub>(piv)<sub>6</sub>(bath)<sub>2</sub>] $\cdot$ 2EtOH (**5a** $\cdot$ 2EtOH) and [Sm<sub>2</sub>(piv)<sub>6</sub>(bath)<sub>2</sub>] $\cdot$ 2EtOH (**5b** $\cdot$ 2EtOH) and terbium complexes [(bath)<sub>2</sub>Tb<sub>2</sub>(piv)<sub>6</sub>] $\cdot$ 1.5EtOH (**6a** $\cdot$ 1.5EtOH) and [Tb<sub>2</sub>(piv)<sub>6</sub>(bath)<sub>2</sub>] (**6b**). Hence, the conclusions about the nature of pivalates **2a** $\cdot$ 1.75EtOH and **2b** $\cdot$ 2EtOH were made based on the comparative study of the thermal behavior of these pivalates and the corresponding samarium complexes **5a** $\cdot$ 2EtOH and **5b** $\cdot$ 2EtOH and terbium complexes **6a** $\cdot$ 1.5EtOH and **6b** before their decomposition (Table 3, Fig. 3). Earlier, we have shown that samarium pivalate [Sm<sub>2</sub>(piv)<sub>6</sub>(bath)<sub>2</sub>] $\cdot$ 2EtOH (**5a** $\cdot$ 2EtOH) undergoes a high-temperature phase transition to form the complex [Sm<sub>2</sub>(piv)<sub>6</sub>(bath)<sub>2</sub>] (**5c**), the molecular and crystal structure of which (X-ray diffraction data) differs from that of **5a** $\cdot$ 2EtOH.<sup>5d</sup> It should be noted that no melting of **5a** $\cdot$ 2EtOH occurred, and what we observed is the melting of **5c** (Table 3, Fig. 3a).<sup>5d</sup> No high-temperature structural phase transition was observed in the solid phase of complex [Tb<sub>2</sub>(piv)<sub>6</sub>(bath)<sub>2</sub>] $\cdot$ 1.5EtOH (**6a** $\cdot$ 1.5EtOH), which differs from [Sm<sub>2</sub>(piv)<sub>6</sub>(bath)<sub>2</sub>] $\cdot$ 2EtOH (**5a** $\cdot$ 2EtOH) by both the structural functions of the  $\mu_2$ -piv anions and the crystal structure. However, **6a** $\cdot$ 1.5EtOH is characterized by its own melting (Fig. 3a).<sup>10</sup> The behavior of heterobimetallic complex [SmTb(piv)<sub>6</sub>(bath)<sub>2</sub>] $\cdot$ 1.75EtOH (**2a** $\cdot$ 1.75EtOH) is similar to that of isostructural complex **5a** $\cdot$ 2EtOH, but the structural phase transition is shifted to lower temperatures (Fig. 3a). For complex [Sm<sub>2</sub>(piv)<sub>6</sub>(bath)<sub>2</sub>] $\cdot$ 2EtOH (**5b** $\cdot$ 2EtOH), complex [Tb<sub>2</sub>(piv)<sub>6</sub>(bath)<sub>2</sub>] (**6b**), and heterobimetallic pivalate [SmTb(piv)<sub>6</sub>(bath)<sub>2</sub>] $\cdot$ 2EtOH (**2b** $\cdot$ 2EtOH), we observed only the melting process. It should be noted that the characteristics of the melting of product **2b** $\cdot$ 2EtOH not additive to the relevant characteristics of the melting of complexes **5b** $\cdot$ 2EtOH and **6b** (Table 3, Fig. 3b). These results provide evidence that pivalates [SmTb(piv)<sub>6</sub>(bath)<sub>2</sub>] $\cdot$ 1.75EtOH (**2a** $\cdot$ 1.75EtOH) and [SmTb(piv)<sub>6</sub>(bath)<sub>2</sub>] $\cdot$ 2EtOH (**2b** $\cdot$ 2EtOH) are individual heterobimetallic complexes. Therefore, the dinuclear lanthanide pivalates with 4,7-diphenyl-1,10-phenanthroline synthesized in the present

study are unique compounds. At high temperatures before the beginning of thermal decomposition, these complexes exhibit a first-order phase transition, namely, the structural phase transition or melting. The characteristics of the latter are known to serve for the identification and also as a criterion of the purity of each individual compound. The above considered approach to the determination of the individuality of coordination compounds of lanthanides was used for the first time.

**Table 2.** Characteristics of the solid-phase thermal decomposition of **1**, **3**, and **4**.

Complex	1 <sup>st</sup> step, °C	$\Delta m \pm 1.5\%$	$t_{\text{end}}$ , °C	$\Sigma \Delta m \pm 1.5\%$	Solid product
<b>1</b>	257 – 340	28.5	480	73.5	amorphous
<b>3</b> <sup>5b</sup>	260 – 330	28.1	485	72.0	Tb <sub>2</sub> O <sub>3</sub>
<b>4</b> <sup>5c</sup>	259 – 361	28.7	480	73.0	Sm <sub>2</sub> O <sub>3</sub>

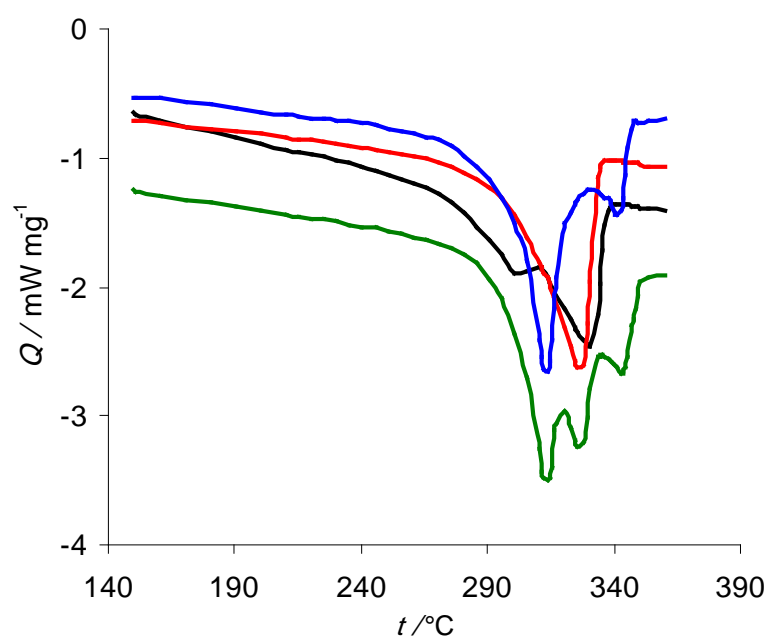
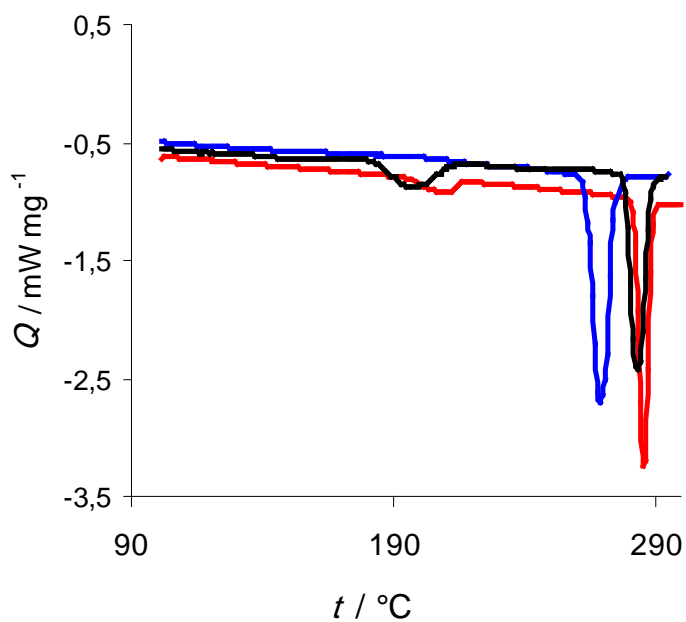
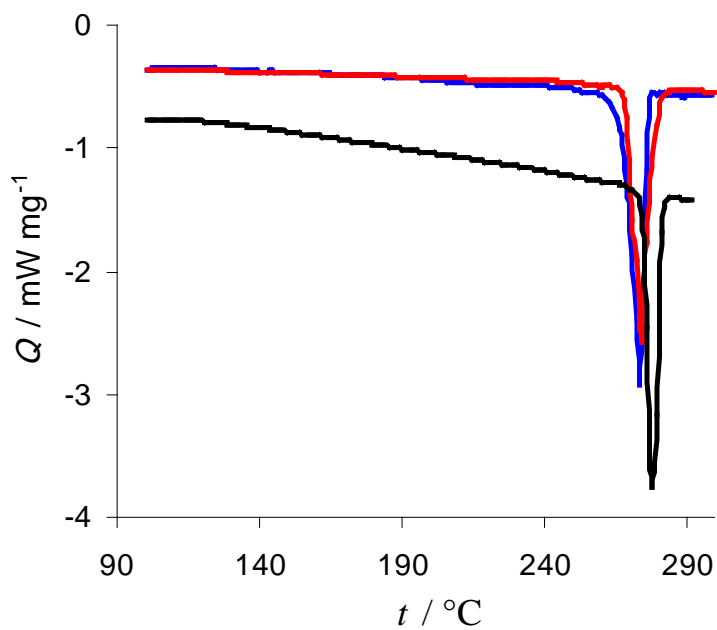


**Fig. 2.** DSC curves for **1** (black), **3** (blue), and **4** (red) and a superposition of the DSC curves for **3** and **4** (green).



a)



b)

**Fig. 3.** DSC curves in the temperature range of 95-295 °C: (a) for **2a**·1.75EtOH (black), **5a**·2EtOH (red), and **6a**·1.5EtOH (blue) and (b) for **2b**·2EtOH (black), **5b**·2EtOH (red), and **6b** (blue).

**Table 3.** Characteristics of the desolvation, melting and phase transitions of complexes **2a**·1.75EtOH, **2b**·2EtOH, **5a**·2EtOH, **5b**·2EtOH, **5c**, **6a**·1.5EtOH, and **6b**.

Complex	Crystal system, space group, V (Å <sup>3</sup> )	t <sub>desolv.</sub> range, °C	t <sub>tr.</sub> , °C	Δ <sub>tr</sub> H <sup>0</sup> , kJ/mol	t <sub>m</sub> , °C	Δ <sub>m</sub> H <sup>0</sup> , kJ/mol
<b>2a</b> ·1.75EtOH	Triclinic, <i>P</i> -1, 4089.5(6)	68 - 112	186.5±1.5	16.5±1.6	—	—
<b>2b</b> ·2EtOH	Monoclinic, <i>C2/c</i> , 8102(3)	67 - 108	—	—	275.4±1.5	98.6± 6.1
<b>5a</b> ·2EtOH <sup>5d</sup>	Triclinic, <i>P</i> -1, 4117.4(6)	66 -105	195.2±1.5	14.7±0.6	—	—
<b>5b</b> ·2EtOH <sup>5d</sup>	Monoclinic, <i>C2/c</i> , 8022(5)	68 -110	—	—	264.8±1.0	94.5±5.0
<b>5c</b> <sup>5d</sup>	Monoclinic, <i>I2/a</i> , 14811.9(12)	—	—	—	281.4±1.0	91.2±4.0
<b>6a</b> ·1.5EtOH <sup>5b</sup>	Triclinic, <i>P</i> -1, 4126.3(5)	65 - 108	—	—	262.5±2.0	98.2± 6.0
<b>6b</b> <sup>10</sup>	Monoclinic, <i>C2/c</i> , 8074.7 (13)	—	—	—	272.1±1.5	104.4± 5.7

### Mass spectrometry

Earlier, we have studied the vaporization of the pivalates [Sm<sub>2</sub>(piv)<sub>6</sub>(Hpiv)<sub>6</sub>],<sup>17</sup> [Ln(piv)<sub>3</sub>]<sub>n</sub> (Ln = Eu,<sup>18</sup> Sm,<sup>17</sup> Tb,<sup>4h</sup> Tm<sup>15d</sup>), and [Ln<sub>2</sub>(piv)<sub>6</sub>(phen)<sub>2</sub>] (Ln<sub>2</sub> = Eu<sub>2</sub>,<sup>18</sup> Sm<sub>2</sub> (**4**),<sup>5d</sup> Tb<sub>2</sub> (**3**),<sup>4h</sup> EuTb<sup>4h</sup>) by the Knudsen effusion method combined with a mass spectrometric analysis of the vaporization products and also studied pivalates [Ln<sub>2</sub>(piv)<sub>6</sub>(bpy)<sub>2</sub>] (Ln<sub>2</sub> = Sm<sub>2</sub>,<sup>5d</sup> Tb<sub>2</sub><sup>10</sup>), [Sm<sub>2</sub>(piv)<sub>6</sub>(bath)<sub>2</sub>]·2EtOH (**5a**·2EtOH),<sup>5d</sup> [Tb<sub>2</sub>(piv)<sub>6</sub>(bath)<sub>2</sub>]·1.5EtOH (**6a**·1.5EtOH),<sup>10</sup> and [Tb<sub>2</sub>(piv)<sub>6</sub>(bath)<sub>2</sub>] (**6b**)<sup>10</sup> by direct inlet probe (DIP) mass spectrometry. It was shown that the dimeric molecules [Ln<sub>2</sub>(piv)<sub>6</sub>] are the main metal-containing component of these compounds in the gas phase, whereas the content of the tetrameric molecules [Ln<sub>4</sub>(piv)<sub>12</sub>] is not higher than 5%.

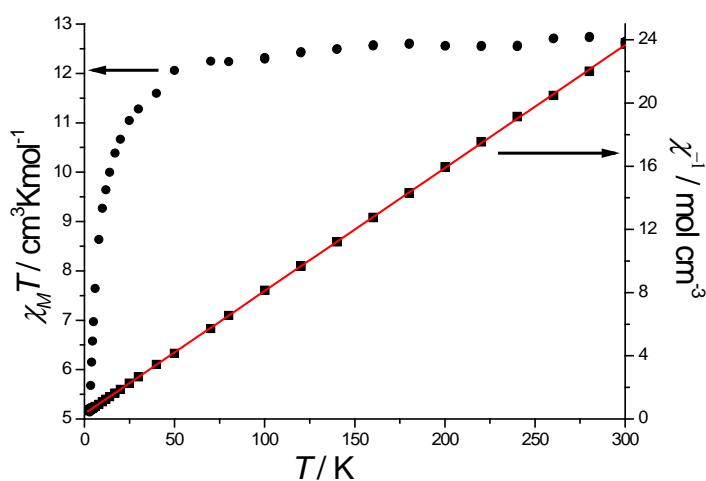
The mass spectra of heterobimetallic pivalates [SmTb(piv)<sub>6</sub>(phen)<sub>2</sub>] (**1**), [SmTb(piv)<sub>6</sub>(bath)<sub>2</sub>]·1.75EtOH (**2a**·1.75EtOH), [SmTb(piv)<sub>6</sub>(bath)<sub>2</sub>]·2EtOH (**2b**·2EtOH), and [SmTb(piv)<sub>6</sub>(bath)<sub>2</sub>]·EtOH (**2b**·EtOH), like the spectra of lanthanide pivalates of similar

composition, show ion peaks at low  $m/z$  corresponding to the fragmentation of phen and bath molecules. This region of the mass spectra is in complete agreement with the data published in the literature:<sup>13</sup> the fragment ion peaks  $(C_{12}H_8N_2)^+$ ,  $(C_{12}H_7N_2)^+$ , and  $(C_{11}H_8N)^+$  are observed for phen;  $(C_{24}H_{16}N_2)^+$ ,  $(C_{24}H_{14}N_2)^+$ ,  $(C_{18}H_{11}N_2)^+$ , and  $(C_6H_5)^+$ , for bath. At  $m/z$  higher than 166 (except for the ion peaks corresponding to the fragmentation of bath), the mass spectrum shows ions containing the metal cation. The mass spectra of compounds **1** and **2a**·1.75EtOH are given in Table S2†. The mass spectra of **2b**·2EtOH and **2b**·EtOH are almost completely identical to the mass spectrum of **2a**·1.75EtOH. These mass spectra characterize the state of samarium terbium *tris*-pivalates in the gas phase. At  $m/z$  higher than 166 (except for the ion peaks corresponding to the fragmentation of bath), the mass spectrum shows ions containing the metal cation. As can be seen from Table S2†, the major part of the ion current accounts for ions containing two different metal atoms. The qualitative and quantitative composition of these ions, as in the case of the complex [EuTb(piv)<sub>6</sub>(phen)<sub>2</sub>], indicates that the [SmTb(piv)<sub>6</sub>] molecules are their molecular precursors. Therefore, under the conditions of the mass spectrometric experiment, the starting compounds undergo decomposition accompanied by the removal of the coordinated neutral ligand, and the *tris*-pivalates exist in the gas phase mainly as [SmTb(piv)<sub>6</sub>] dimers.

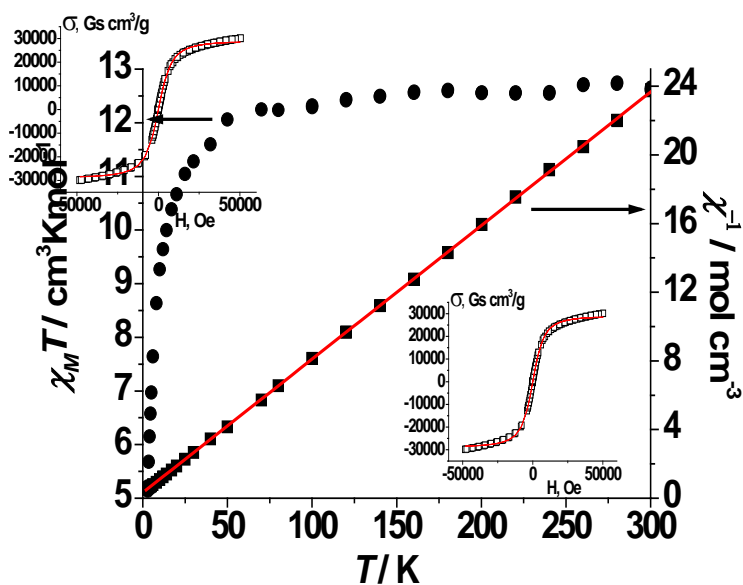
### Magnetic properties

The magnetic characteristics of samarium and terbium complexes [Tb<sub>2</sub>(piv)<sub>6</sub>(phen)<sub>2</sub>] (**3**), [Sm<sub>2</sub>(piv)<sub>6</sub>(phen)<sub>2</sub>] (**4**), [Sm<sub>2</sub>(piv)<sub>6</sub>(bath)<sub>2</sub>]·2EtOH (**5a**·2EtOH), and [Tb<sub>2</sub>(piv)<sub>6</sub>(bath)<sub>2</sub>]·1.5EtOH (**6a**·1.5EtOH) were reported earlier.<sup>5b,5d</sup> The temperature dependences  $\chi_M T$  (●) and  $1/\chi$  for heterobimetallic pivalates [SmTb(piv)<sub>6</sub>(phen)<sub>2</sub>] (**1**) and [SmTb(piv)<sub>6</sub>(bath)<sub>2</sub>]·1.75EtOH (**2a**·1.75EtOH) are displayed in Fig. 4. In the temperature range of 70-300 K, the plots  $1/\chi(T)$  for pivalates **1** and **2a**·1.75EtOH, like those for the corresponding terbium complexes **3** and **6a**·1.5EtOH,<sup>5b</sup> are linear and are well-described by the Curie-Weiss equation. This is accounted for by the fact that Tb<sup>3+</sup> ions make the major contribution to the magnetic susceptibility of pivalates **1** and **2a**·1.75EtOH. The optimal values of the Curie constant  $C$  and the Weiss constant  $\theta$  are 12.85 cm<sup>3</sup>·K/mol and -4.14 K for **1** and 12.71 cm<sup>3</sup>·K/mol and -4.71 K for **2a**·1.75EtOH. The Curie constants  $C$  estimated for **1** and **2a**·1.75EtOH are somewhat larger than the theoretical value (11.81 cm<sup>3</sup>·K/mol) for one Tb<sup>3+</sup> ion (ground state <sup>7</sup>F<sub>6</sub> and  $g_J = 3/2$ ) because Sm<sup>3+</sup> ions (ground state <sup>6</sup>H<sub>5/2</sub> and  $g_J = 2/7$ ) also contribute to the paramagnetism of the complexes. The values of  $\chi_M T$  at 300 K are 12.61 and 12.62 cm<sup>3</sup> K/mol for **1** and **2a**·1.75EtOH, respectively, and they are in good agreement

with the value of  $12.05 \text{ cm}^3 \text{ K/mol}$  obtained by the summation of the contributions of equal amounts of  $\text{Sm}^{3+}$  and  $\text{Tb}^{3+}$  ions to the magnetic susceptibility. The ground state of  $\text{Sm}^{3+}$  ions is  $^6H_{5/2}$  and  $g_J = 2/7$ , but there are closely lying levels with different  $J$  states, the population of which varies substantially with temperature. The electronic structure of the  $\text{Sm}^{3+}$  ion and the zero-field splitting typical of the  $\text{Tb}^{3+}$  ion are responsible for a decrease in  $\chi_M T$  with decreasing temperature. It should be noted that the dependence of the magnetization on the external magnetic field for complex **2a**·1.75EtOH at 2 K, as opposed to that for terbium complex **6a**·1.5EtOH, is nonlinear (Fig. 4b, insert) and is well-described by the Brillouin function with the parameters  $J$  and  $g$  equal to 4.31 and 1.13, respectively.



a)



b)

**Fig. 4.** Plots  $\chi_M T(T)$  (●) and  $1/\chi(T)$  (■) for **1** (a) and for **2a**·1.75EtOH (insert: plot  $\sigma(H)$ ) (b), calculated data are represented by the red line.

### Photoluminescence properties

Photoluminescence of homonuclear lanthanide complexes with organic ligands is still being actively studied. For many known compounds, excitation energy relaxation processes between ligand levels and between levels of ligands and the  $\text{Ln}^{3+}$  ion have been investigated in sufficient detail<sup>1g, 3a, 19</sup> However, systems with different lanthanide atoms, such as solid solutions, statistical mixtures, and, much more rarely, individual compounds, are little studied. It should be noted that these systems are, as a rule, bimetallic and most of them contain Eu-Tb,<sup>4e, 20</sup> Nd-Tb,<sup>21</sup> or Eu-Yb.<sup>4a</sup> The presence of terbium ions in such systems usually aids in enhancing PL of the second lanthanide ion *via* the so-called energy-cascade mechanism, as well as due to a decrease in the efficiency of self-quenching. As a consequence, such systems often exhibit intense photoluminescence in the visible range and are of potential interest in the design of luminescent materials and devices based on these materials. The results of systematic studies of the mechanisms of energy transfer between different lanthanide ions were reported in the publications.<sup>22, 4e, 4h</sup> However, such studies were virtually not performed for Sm-Tb systems.<sup>4c, 22</sup> The present work is a continuation of our earlier systematic studies<sup>5b, 5d</sup> of the PL properties of homo- and heterodinuclear pivalates with  $\text{Sm}^{3+}$  and  $\text{Tb}^{3+}$  atoms and the chelating heterocyclic N-donors bath and phen.

To interpret the PL spectra of complexes  $[\text{SmTb}(\text{piv})_6(\text{phen})_2]$  (**1**),  $[\text{SmTb}(\text{piv})_6(\text{bath})_2] \cdot 1.75\text{EtOH}$  (**2a**·1.75EtOH),  $[\text{Tb}_2(\text{piv})_6(\text{phen})_2]$  (**3**),  $[\text{Sm}_2(\text{piv})_6(\text{phen})_2]$  (**4**),  $[\text{Sm}_2(\text{piv})_6(\text{bath})_2] \cdot 2\text{EtOH}$  (**5a**·2EtOH), and  $[\text{Tb}_2(\text{piv})_6(\text{bath})_2] \cdot 1.5\text{EtOH}$  (**6a**·1.5EtOH) we determined the positions of the singlet ( $S_1$ ) levels of the bath and phen ligands. In the present study, we measured the PL and scattering spectra of known gadolinium pivalates with these ligands<sup>5b</sup>  $[\text{Gd}_2(\text{piv})_6(\text{bath})_2]$  (**7**) and  $[\text{Gd}_2(\text{piv})_6(\text{phen})_2]$  (**8**), respectively, in order to determine the positions of the  $S_1$  levels of the bath and phen ligands. Fig. S2† displays the PL and scattering spectra for **7** and presents the method used for the calculation of the position of the  $S_1$  energy level of the bath ligand employing the law of mirror symmetry (Levshin rule<sup>23</sup>). This method gave  $\sim 27450 \text{ cm}^{-1}$  (364 nm) and  $\sim 27980 \text{ cm}^{-1}$  (357 nm) for the  $S_1$  levels of the bath and phen ligands, respectively. Fig. 5 shows the energy-level scheme for **1**, **2a**·1.75EtOH, **3**, **4**, **5a**·2EtOH, and **6a**·1.5EtOH. The positions of the  $T_1$  triplet levels

( $\sim 20830\text{ cm}^{-1}$  (480 nm) for bath and  $22100\text{ cm}^{-1}$  (452 nm) for phen) were determined in the study;<sup>5b</sup> the positions of the  $4f$  levels of  $\text{Ln}^{3+}$  ions were taken from the work.<sup>24</sup>

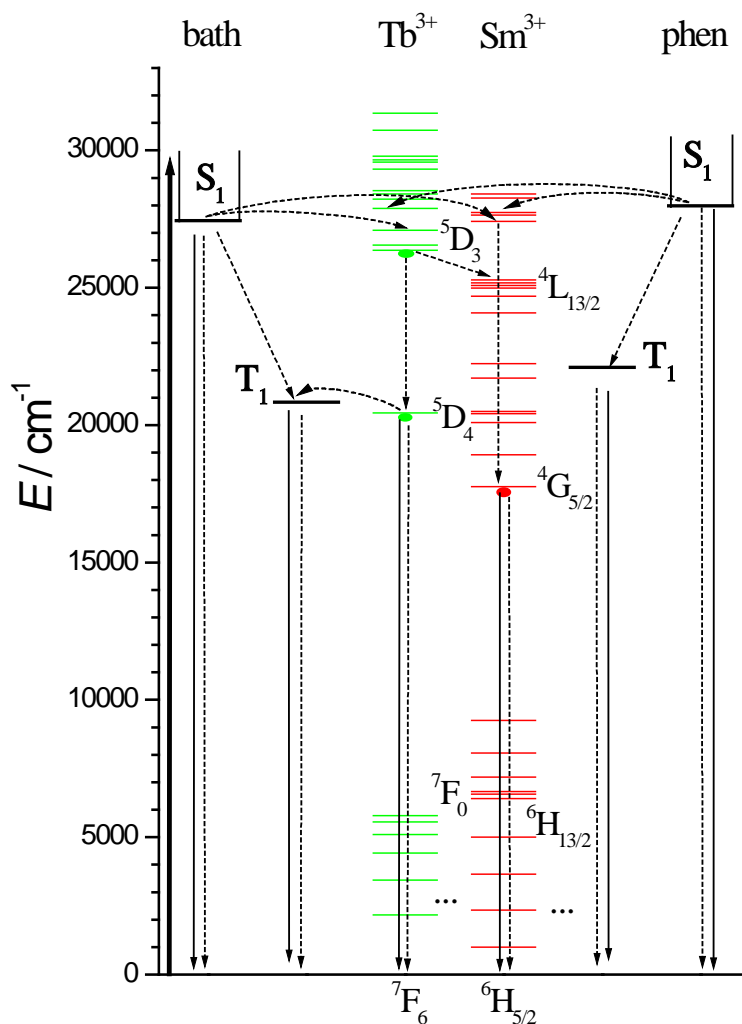


**Fig. 5.** Chart of the main processes of energy transfer between the levels of the bath and phen ligands and the  $\text{Tb}^{3+}$  and  $\text{Sm}^{3+}$  ions in **1**, **2a**·1.75EtOH, **3**, **4**, **5a**·2EtOH, and **6a**·1.5EtOH. An oval indicates that the level is metastable.

The PL spectra of heterobimetallic complexes  $[\text{SmTb}(\text{piv})_6(\text{phen})_2]$  (**1**) and  $[\text{SmTb}(\text{piv})_6(\text{bath})_2]\cdot 1.75\text{EtOH}$  (**2a**·1.75EtOH) and related samarium and terbium complexes  $[\text{Tb}_2(\text{piv})_6(\text{phen})_2]$  (**3**),  $[\text{Sm}_2(\text{piv})_6(\text{phen})_2]$  (**4**),  $[\text{Sm}_2(\text{piv})_6(\text{bath})_2]\cdot 2\text{EtOH}$  (**5a**·2EtOH), and  $[\text{Tb}_2(\text{piv})_6(\text{bath})_2]\cdot 1.5\text{EtOH}$  (**6a**·1.5EtOH)<sup>5b,5d</sup> measured at 300 and 77 K are displayed in Figures 6 and 7. Under UV excitation ( $\lambda_{\text{ex}} = 337\text{ nm}$ ), the spectra of terbium complexes **3** and **6a**·1.5EtOH and samarium complexes **4** and **5a**·2EtOH show narrow PL bands characteristic of the  $\text{Tb}^{3+}$  ( $^5\text{D}_4 \rightarrow ^7\text{F}_J$ , J

= 2-6) and  $\text{Sm}^{3+}$  ( $^4\text{G}_{5/2} \rightarrow ^6\text{H}_j$ ,  $J = 5/2-11/2$ ) electron transitions, respectively. The spectra of complexes **1** and **2a**·1.75EtOH show narrow PL bands of two types of ions, but **1** and **2a**·1.75EtOH emit in the red at 300 K because the  $\text{Sm}^{3+}$  ions PL is more intense than the PL of  $\text{Tb}^{3+}$  ions. The spectra of samarium complexes **4** and **5a**·2EtOH measured at 300 K exhibit, along with narrow PL bands of lanthanide ions, broad PL bands in the near-UV range with a maximum at 380-390 nm are assigned to singlet-singlet transitions ( $\text{S}_1 \rightarrow \text{S}_0$ ) of the bath and phen ligands, respectively (Figs. 6b and 7b). It should be noted that the intensity of the singlet PL band depends on the type of the ligand. In samarium pivalate **5a**·2EtOH with the bath ligand, the  $\text{S}_1 \rightarrow \text{S}_0$  transition is the most efficient one.

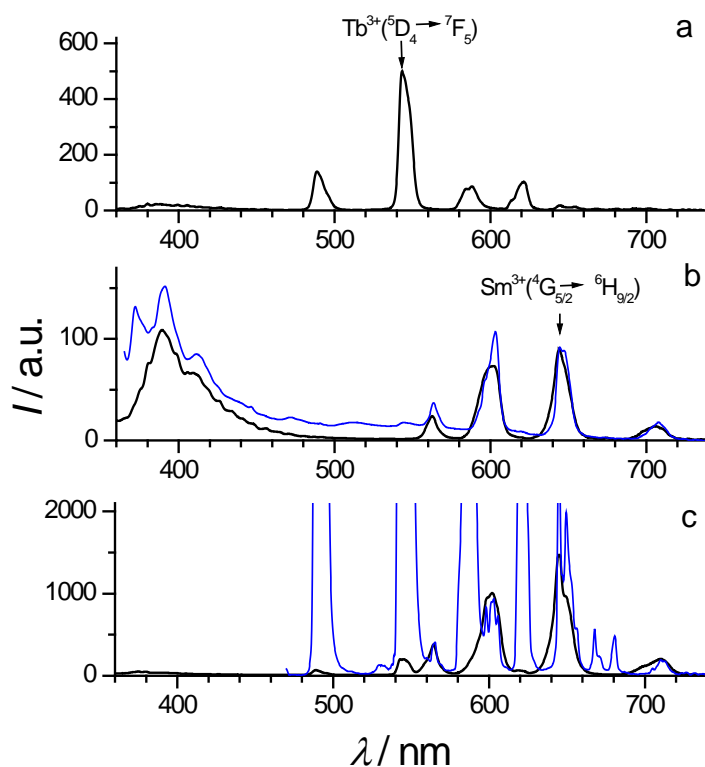


**Fig. 6.** PL spectra ( $\lambda_{ex} = 337$  nm; black, 300 K; blue, 77 K): (a) **6a**·1.5EtOH, (b) **5a**·2EtOH, (c) **2a**·1.75EtOH.

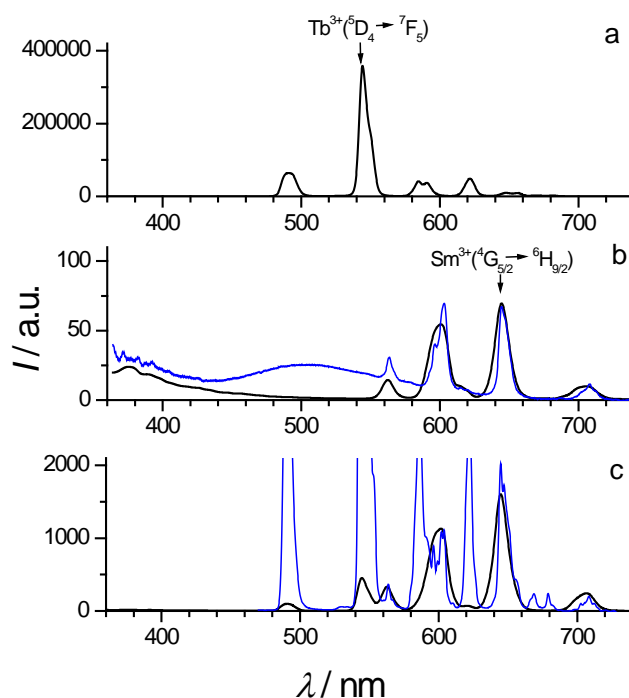


**Fig. 7.** PL spectra ( $\lambda_{ex} = 337$  nm; black, 300 K; blue, 77 K): (a) **3**, (b) **4**, (c) **1**.

This fact is confirmed by the PL spectra of gadolinium complexes **7** and **8** (Fig. S3†), which show only PL of the ligand because  $Gd^{3+}$  ions have no effect. As can be seen from Figure S3b†, the internal  $S_1 \rightarrow T_1$  conversion in phen is so much efficient that the PL band originating from the  $S_1 \rightarrow S_0$  transition is virtually absent at both temperatures. As can be seen from Figures 6b and 7b, the PL intensity of  $Sm^{3+}$  ions in  $[Sm_2(piv)_6(bath)_2] \cdot 2EtOH$  (**5a**·2EtOH) is somewhat higher than that in  $[Sm_2(piv)_6(phen)_2]$  (**4**). In addition, the PL intensity of  $Sm^{3+}$  ions is the same at 77 and 300 K, whereas the PL intensity of the  $T_1$  level of the bath and phen ligands is obviously higher at 77 K. From this it follows that the relaxation channel from the  $T_1$  excited state to the  $4f$  levels of  $Sm^{3+}$  ions is not the major one. This suggests that the excitation energy transfer occurs *via* the scheme  $S_1 \rightarrow 4f(Sm^{3+})$ , as shown in Figure 5. Therefore,  $K_{rel}(i) \cdot \xi$  for  $Sm^{3+}$  ions in **4** is 20% smaller than that in **5a**·2EtOH (Table 1) due to the more efficient internal  $S_1 \rightarrow T_1$  conversion in **4** compared to **5a**·2EtOH. It should be noted that the PL decay kinetics for **4** and **5a**·2EtOH measured at  $\lambda = 601$  nm is the same at both temperatures, and the PL decay times are not longer than  $\tau_{300, 77 K} \leq 0.017$  ms (Table 4). Such short times are indicative of the Sm-Sm intramolecular quenching of  $Sm^{3+}$  ions due to the presence of two identical energy-state systems. This quenching is most pronounced for luminescence levels having low luminous efficiency. It is known that in crystals at 10 K, the PL

decay time of the  ${}^4G_{5/2}$  level of  $Sm^{3+}$  ions is  $\tau_r = 2.16$  ms.<sup>24</sup> In heterobimetallic complexes  $[SmTb(piv)_6(phen)_2]$  (**1**) and  $[SmTb(piv)_6(bath)_2] \cdot 1.75EtOH$  (**2a**·1.75EtOH), in which the Sm-Sm intramolecular quenching is absent, the PL decay time is  $\tau = 0.06$  ms at 300 K (Table 4). Therefore, the maximum efficiency of radiative relaxation of the  ${}^4G_{5/2}$  level can be estimated at  $\tau/\tau_r = 2.8\%$ . A similar quenching mechanism was observed in the study,<sup>20</sup> in which it was noted that this mechanism is more efficient for  $Sm^{3+}$  ions compared with  $Tb^{3+}$  ions, which is explained from the standpoint of high efficiency of luminescence of  $Tb^{3+}$  ions ( $\tau/\tau_r = 89.7\%$ , where  $\tau_r = 1.45$  ms<sup>24</sup>).

**Table 4.** PL decay times ( $\tau$ ) of the  ${}^4G_{5/2} \rightarrow {}^6H_{7/2}$  and  ${}^5D_4 \rightarrow {}^7F_6$  transitions of  $Sm^{3+}$  and  $Tb^{3+}$  ions in complexes **1**, **2a**·1.75EtOH, **3**, **4**, **5a**·2EtOH, and **6a**·1.5EtOH.

Complex	$\tau_{77\text{ K}}$ , ms		$\tau_{300\text{ K}}$ , ms	
	$Sm^{3+}$	$Tb^{3+}$	$Sm^{3+}$	$Tb^{3+}$
<b>1</b>	0.07±0.02	1.3±0.02	0.06±0.02	0.1±0.02
<b>2a</b> ·1.75EtOH	0.06±0.02	1.3±0.02	0.06±0.02	≤0.017
<b>3</b>	-	1.1±0.02	-	1.1±0.02
<b>4</b>	≤0.017	-	≤0.017	-
<b>5a</b> ·2EtOH	≤0.017	-	≤0.017	-
<b>6a</b> ·1.5EtOH	-	1.2±0.02	-	0.08±0.02 ≤0.017

As opposed to samarium complexes  $[Sm_2(piv)_6(phen)_2]$  (**4**) and  $[Sm_2(piv)_6(bath)_2] \cdot 2EtOH$  (**5a**·2EtOH), the PL intensity of  $Tb^{3+}$  ions in terbium complexes  $[Tb_2(piv)_6(phen)_2]$  (**3**) and  $[Tb_2(piv)_6(bath)_2] \cdot 1.5EtOH$  (**6a**·1.5EtOH) depends substantially on the type of the N-donor ligand (Figs. 6a and 7a). For complex **3**, the  $Tb^{3+}$  ions PL amplitude, like the decay kinetics, which will be discussed below, is the same at 77 and 300 K. This is evidence that the relaxation channel for excitation energy from the  $T_1$  state to the 4f levels of  $Tb^{3+}$  ions as in the case of  $Sm^{3+}$  ions (see above), is not the major one. In related terbium complexes, as in complexes **4** and **5a**·2EtOH, the excitation energy relaxation occurs *via* the scheme  $S_1 \rightarrow 4f(Tb^{3+})$ .<sup>4h,25</sup> The weak PL intensity of  $Tb^{3+}$  ions in **6a**·1.5EtOH compared to **3** may be associated with PL quenching of  $Tb^{3+}$  ions in this complex through the conversion of excited states to the  $T_1$  level of the bath ligand lying close to the metastable  ${}^5D_4$  level (Fig. 5). As can be seen from Table 1,  $K_{rel}(i) \cdot \xi$  for  $Tb^{3+}$  ions in **3** is 600 times

larger than that for **6a**·1.5EtOH. Measurements of the kinetics of PL (see Table 1) showed that  $\tau_{77,300\text{ K}} = 1.1 \pm 0.02$  ms for **3**. For **6a**·1.5EtOH, the time  $\tau_{77\text{ K}} = 1.2 \pm 0.02$  ms, but at room temperature the PL decay kinetics is not monoexponential and is substantially more rapid ( $\tau'_{300\text{ K}} = 0.08 \pm 0.02$  ms and  $\tau^2_{300\text{ K}} \leq 0.017$  ms), the amplitudes of the PL kinetic curves for  $\text{Tb}^{3+}$  ions in **6a**·1.5EtOH being equal to those for  $\text{Tb}^{3+}$  ions in **3**, which is indicative of the  $^5\text{D}_4 \rightarrow \text{T}_1$  excited state conversion. The values of the times  $\tau_{300\text{ K}}$  provide an estimate for the relative efficiency of the  $\text{L} \rightarrow \text{Tb}^{3+}$  relaxation channel for the bath and phen ligands. The efficiency of radiative relaxation from the  $^5\text{D}_4$  level of  $\text{Tb}^{3+}$  ions in **6a**·1.5EtOH is not more than  $\frac{\tau_{300\text{ K}}^{(3)}}{\tau_{300\text{ K}}^{(6a \cdot 1.5\text{EtOH})}} \approx 15$  times weaker than that in complex **3**. However, in the case of the 600-fold difference between  $K_{rel(i)} \cdot \xi$  of  $\text{Tb}^{3+}$  ions in **6a**·1.5EtOH and **3**, the efficiencies of the  $\text{L} \rightarrow \text{Tb}^{3+}$  relaxation channel should differ at least 40-fold. Therefore, it can be stated that the more than two orders of magnitude difference in the PL intensity of  $\text{Tb}^{3+}$  ions is attributed both to the less efficient excitation energy relaxation from the bath ligand to the metal atom and the PL quenching of  $\text{Tb}^{3+}$  ions due to the presence of the  $\text{T}_1$  level of the bath ligand lying close to the metastable  $^5\text{D}_4$  level.

An analysis of the data for heterobimetallic complexes  $[\text{SmTb}(\text{piv})_6(\text{phen})_2]$  (**1**) and  $[\text{SmTb}(\text{piv})_6(\text{bath})_2] \cdot 1.75\text{EtOH}$  (**2a**·1.75EtOH) (Figs. 6c and 7c, Table 1) shows that  $K_{rel(i)} \cdot \xi$  for  $\text{Sm}^{3+}$  ions in these compounds are 20 and 14 times larger than in the corresponding samarium complexes  $[\text{Sm}_2(\text{piv})_6(\text{phen})_2]$  (**4**) and  $[\text{Sm}_2(\text{piv})_6(\text{bath})_2] \cdot 2\text{EtOH}$  (**5a**·2EtOH). In addition, the PL decay time of  $\text{Sm}^{3+}$  ions in **1** and **2a**·1.75EtOH increases by at least 3.5 times (Table 4). These changes are apparently associated with the presence of  $\text{Tb}^{3+}$  ions in these compounds. First, the increase in the PL decay time may be due to the absence of the above-mentioned Sm-Sm intramolecular quenching of  $\text{Sm}^{3+}$  ions. Second, the excitation energy transfer can occur *via* the scheme  $\text{S}_1 \rightarrow 4f(\text{Tb}^{3+}) \rightarrow 4f(\text{Sm}^{3+})$  (Fig. 5) similar to that observed for the dinuclear complex  $[\text{EuTb}(\text{piv})_6(\text{phen})_2]$ .<sup>4h</sup> To confirm the latter statement, we measured excitation spectra of  $[\text{SmTb}(\text{piv})_6(\text{phen})_2]$  (**1**),  $[\text{SmTb}(\text{piv})_6(\text{bath})_2] \cdot 1.75\text{EtOH}$  (**2a**·1.75EtOH), and  $[\text{Tb}_2(\text{piv})_6(\text{phen})_2]$  (**3**) (Fig. 8). The PL excitation spectra of heterobimetallic **1** and **2a**·1.75EtOH show bands of  $\text{Sm}^{3+}$  ions and the  $^7\text{F}_6 \rightarrow ^5\text{D}_3$  transition of  $\text{Tb}^{3+}$  ions, while the excitation band due to the  $^7\text{F}_6 \rightarrow ^5\text{D}_4$  transition of  $\text{Tb}^{3+}$  ions is absent. This is evidence that the excitation energy transfer to  $\text{Tb}^{3+}$  ions occurs *via* the singlet level  $\text{S}_1$  rather than *via* the triplet level  $\text{T}_1$ . It should be noted that the PL intensity of  $\text{Sm}^{3+}$  ions in heterobimetallic complexes **1** and **2a**·1.75EtOH, like in samarium complexes  $[\text{Sm}_2(\text{piv})_6(\text{phen})_2]$  (**4**) and  $[\text{Sm}_2(\text{piv})_6(\text{bath})_2] \cdot 2\text{EtOH}$  (**5a**·2EtOH), is virtually independent of the

type of the ligand. On the other hand, the presence of  $\text{Sm}^{3+}$  ions both in **1** and **2a**·1.75EtOH leads to an efficient PL quenching of  $\text{Tb}^{3+}$  ions, to be more precise, PL from the  $^5\text{D}_4$  level. In **1** and **2a**·1.75EtOH, the PL decay time of  $\text{Tb}^{3+}$  ions at 300 K decreases by at least 11 and 4.7 times, respectively, compared to the PL decay time of  $\text{Tb}^{3+}$  ions in  $[\text{Tb}_2(\text{piv})_6(\text{phen})_2]$  (**3**) and  $[\text{Tb}_2(\text{piv})_6(\text{bath})_2]$ ·1.5EtOH (**6a**·1.5EtOH) (Table 4). As the temperature decreases to 77 K, the PL decay times in **1** and **2a**·1.75EtOH become equal to each other and increase to 1.3 ms, which is accompanied by a considerable increase in the PL intensity of  $\text{Tb}^{3+}$  ions in **1** and **2a**·1.75EtOH, by 40 and 100 times, respectively, comparing with 300 K (Figs. 6c and 7c). The PL color evidently changes from red at 300 K to bright green at 77 K. However, it was experimentally found (Figs. 6c and 7c) that the PL amplitudes of  $\text{Sm}^{3+}$  ions in **1** and **2a**·1.75EtOH remain unchanged and, consequently, the PL quenching of  $\text{Tb}^{3+}$  ions is not due to the direct excitation energy transfer from the  $^5\text{D}_4$  level of  $\text{Tb}^{3+}$  ions to the  $4f$  levels of  $\text{Sm}^{3+}$ . This result was unexpected, because, for example, the calculated radiative lifetimes of the  $^5\text{D}_4$  level is more than one-and-a-half times longer than that of the  $^5\text{D}_3$  level for  $\text{TbF}_3$ .<sup>24</sup> Moreover the  $\text{Sm}^{3+}$  ion having levels comparable in energy with the  $^5\text{D}_4$  level. The excitation energy transfer from the  $^5\text{D}_4$  level, for example, to  $\text{Sm}^{3+}$  or  $\text{Eu}^{3+}$  was observed.<sup>4c, 4e</sup>

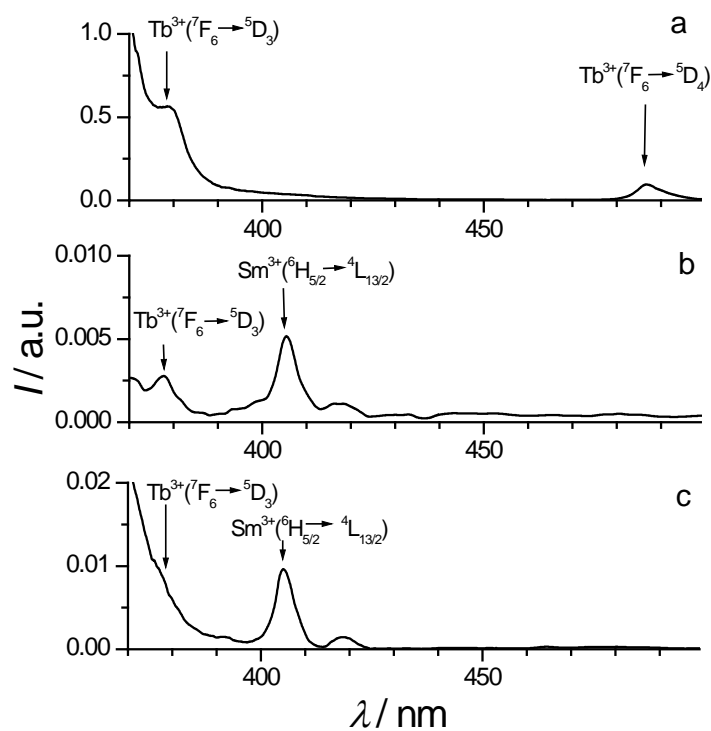


**Fig. 8.** PL excitation spectra (300 K): (a) **3** ( $\lambda_{obs} = 545$  nm), (b) **1** ( $\lambda_{obs} = 645$  nm), (c) **2a**·1.75EtOH ( $\lambda_{obs} = 645$  nm).

## Conclusions

To summarize, we synthesized new heterobimetallic pivalates [SmTb(piv)<sub>6</sub>(phen)<sub>2</sub>] (**1**), [SmTb(piv)<sub>6</sub>(bath)<sub>2</sub>]·1.75EtOH (**2a**·1.75EtOH), [SmTb(piv)<sub>6</sub>(bath)<sub>2</sub>]·2EtOH (**2b**·2EtOH), and [SmTb(piv)<sub>6</sub>(bath)<sub>2</sub>]·EtOH (**2b**·EtOH), which are individual compounds containing chelating N-donor phen or bath molecules as neutral ligands. Complexes **2a**·2EtOH and **2b**·2EtOH differ by the structural functions of the bridging piv anions (two  $\mu_2$ -piv- $\kappa^2$ O,O,O' and two  $\mu_2$ -piv- $\kappa^2$ O,O' anions in **2a**·1.75EtOH and four  $\mu_2$ -piv- $\kappa^2$ O,O' anions in **2b**·2EtOH and **2b**·EtOH) and have different molecular and crystal structures. The thermal stability of heterobimetallic SmTb pivalates, like that of Sm, Eu, Tb, and EuTb compounds of similar composition, increases with the replacement of coordinated phen molecules by bath. The unique feature of the thermal behavior at high temperatures before thermal decomposition of complexes **2a**·1.75EtOH and **2b**·2EtOH, as well as of the known complexes [Ln<sub>2</sub>(piv)<sub>6</sub>(bath)<sub>2</sub>]·xSolv (Ln = Eu, Sm, Tb,  $x = 0-2$  and Solv = EtOH or H<sub>2</sub>O),<sup>5b,5d,10</sup> is that these complexes exhibit first-order phase transitions, namely, the structural phase transition, or melting. The above-considered thermal analytical approach to the determination of the individuality of coordination compounds of lanthanide is an original method. Under the conditions of the mass spectrometric experiment, compounds **1**, **2a**·1.75EtOH, **2b**·2EtOH, and **2b**·EtOH undergo decomposition accompanied by elimination of the coordinated N-donor ligand, and tris-pivalates exist predominantly as [SmTb(piv)<sub>6</sub>] dimers in the gas phase. The magnetochemical study shows that the magnetic properties of **1** and **2a**·1.75EtOH are mainly determined by the Tb<sup>3+</sup> ions, and a decrease in  $\chi_M T$  with decreasing temperature is caused by the zero-field splitting. The spectroscopic studies showed that the internal S<sub>1</sub>→T<sub>1</sub> conversion is more efficient for the phen ligand than for the bath ligand. In addition, the intercombination conversion of the excited states L→Tb<sup>3+</sup> in [Tb<sub>2</sub>(piv)<sub>6</sub>(phen)<sub>2</sub>] (**3**) is 40 times more efficient than that in [Tb<sub>2</sub>(piv)<sub>6</sub>(bath)<sub>2</sub>]·1.5EtOH (**6a**·1.5EtOH). In homobimetallic complexes [Tb<sub>2</sub>(piv)<sub>6</sub>(phen)<sub>2</sub>] (**3**), [Sm<sub>2</sub>(piv)<sub>6</sub>(phen)<sub>2</sub>] (**4**), [Sm<sub>2</sub>(piv)<sub>6</sub>(bath)<sub>2</sub>]·2EtOH (**5a**·2EtOH), and [Tb<sub>2</sub>(piv)<sub>6</sub>(bath)<sub>2</sub>]·1.5EtOH (**6a**·1.5EtOH), the excited state relaxation occurs *via* the scheme S<sub>1</sub>→4f(Sm<sup>3+</sup>, Tb<sup>3+</sup>). The involvement of the T<sub>1</sub> level is manifested only in **6a**·1.5EtOH, only the quenching of the luminescence level <sup>5</sup>D<sub>4</sub>(Tb<sup>3+</sup>)→T<sub>1</sub> being observed. It was experimentally found that the presence of Tb<sup>3+</sup> ions in **1** and **2a**·1.75EtOH leads to

an increase in the efficiency of luminescence of  $\text{Sm}^{3+}$  ions by at least an order of magnitude, this increase is comparable in both complexes and is not associated with the direct excitation energy transfer  $4f(\text{Tb}^{3+}) \rightarrow 4f(\text{Sm}^{3+})$ . The presence of  $\text{Sm}^{3+}$  ions leads to a decrease in the efficiency of luminescence of  $\text{Tb}^{3+}$  ions by a factor of 3.5 in **2a**·1.75EtOH and 800-fold in **1**. This is due to the excitation energy transfer  ${}^5\text{D}_3(\text{Tb}^{3+}) \rightarrow 4f(\text{Sm}^{3+})$  and also to an increase in the efficiency of nonradiative excited state relaxation channel from the  ${}^5\text{D}_4(\text{Tb}^{3+})$  level. It was shown that the PL quenching of  $\text{Tb}^{3+}$  ions in **1** and **2a**·1.75EtOH is not associated with the direct excitation energy transfer  ${}^5\text{D}_4(\text{Tb}^{3+}) \rightarrow 4f(\text{Sm}^{3+})$ . As the temperature decreases to 77 K, the PL decay times of  $\text{Tb}^{3+}$  ions in **1** and **2a**·1.75EtOH become equal to each other and increases to 1.3 ms, which is accompanied by a considerable increase in the PL intensity of  $\text{Tb}^{3+}$  ions in **1** and **2a**·1.75EtOH by 40 and 100 times, respectively, compared to 300 K. The PL color evidently changes from red at 300 K to bright green at 77 K. Therefore, the above-described results suggest that compounds **1** and **2a**·1.75EtOH can be considered as potential functional components of new luminescent sensor devices.

## Acknowledgments

This study was supported by the Russian Foundation for Basic Research (Project Nos. 13-03-00470, 12-03-00627, 14-03-00463, 13-03-00408, and 13-03-12428), the Council on Grants at the President of the RF (Program for Support of Leading Scientific Schools, Grants NSh-1712.2014.3 and NSh-4773.2014.3), and the Russian Academy of Science.

## References

- (a) K. Binnemans, *Chem. Rev.*, 2009, **109**, 4283–4374; (b) C.-H. Huang, *Rare Earth Coordination Chemistry: Fundamentals and Applications*, John Wiley & Sons Pte Ltd, Singapore, 2010; (c) D. Gatteschi, R. Sessoli, J. Villain, *Molecular nanomagnets*, Oxford University Press, Oxford, 2006; (d) K. Bernot, L. Bogani, A. Caneschi, D. Gatteschi, R. Sessoli, *J. Am. Chem. Soc.*, 2006, **128**, 7947–7956; (e) B. Yan, Y.-F. Shao, *Dalton Trans.*, 2013, **42**, 9565–9573; (f) A. Cornia, M. Mannini, P. Saintavrit, R. Sessoli, *Chem. Soc. Rev.*, 2011, **40**, 3076–3091; (g) S. V. Eliseeva, J.-C. G. Bunzli, *Chem. Soc. Rev.*, 2010, **39**, 189–227; (h) H.L. Jiang, Q. Xu, *Chem. Commun.*, 2011, **47**, 3351–3370; (i) A. Corma, H. Garcia, F.X. Llabres i Xamena, *Chem. Rev.*, 2010, **110**, 4606–4655.

- 2 (a) T. Ishiwata, Y. Furukawa, K. Sugikawa, K. Kokado, K. Sada, *J. Am. Chem. Soc.*, 2013, **135**, 5427–5432; (b) J. Xu, J. W. Cheng, W. P. Su, M. C. Hong, *Cryst. Growth Des.*, 2011, **11**, 2294–2301; (c) J. Z. Gu, J. Wu, D. Y. Lv, Y. Tang, K. Zhu, J. Wu, *Dalton Trans.*, 2013, **42**, 4822–4830; (d) J. M. Tian, B. Li, X. Y. Zhang, X. L. Li, J. P. Zhang, *Dalton Trans.*, 2013, **42**, 8504–8511; (e) M. Sugita, N. Ishikawa, T. Ishikawa, S. Koshihara, Y. Kaizu, *Inorg. Chem.*, 2006, **45**, 1299–1304; (f) E. Coronado, C. Gimenez-Saiz, A. Recuenco, A. Tarazon, F. M. Romero, A. Camon, F. Luis, *Inorg. Chem.*, 2011, **50**, 7370–7372; (g) X. Feng, X. L. Ling, L. Liu, H. L. Song, L. Y. Wang, S. W. Ng, B. Y. Su, *Dalton Trans.*, 2013, **42**, 10292–10303.
- 3 G. F. De Sa, O. L. Malta, C. De Mello Donega, A. M. Simas, R. L. Longo, P. A. Santa-Cruz, da E. F. Silva, *Coord. Chem. Rev.*, 2000, **196**, 165–195; (b) J.-C. G. Bünzli, C. Piguet, *Chem. Soc. Rev.*, 2005, **34**, 1048–1077; (c) J.-C. G. Bünzli, C. Piguet, *Chem. Rev.*, 2002, **102**, 1897–1928; (d) D. Parker, *Coord. Chem. Rev.*, 2000, **205**, 109–130.
- 4 (a) M. A. Singh-Wilmot, I. A. Kahwa, A. J. P. White, D. J. Williams, A. J. Lough, *Polyhedron*, 2010, **29**, 270–279; (b) M. Lee, M. S. Tremblay, S. Jockusch, N. J. Turro, D. Sames, *Org. Lett.* 2011, **13**, 2802–2805; (c) B. Han, H. Liang, Y. Huang, Y. Tao, Q. Su, *Appl. Phys. B*, 2011, **104**, 241–246; (d) P. C. R. Soares-Santos, L. Cunha-Silva, F. A. A. Paz, R. A. S. Ferreira, T. Trindade, L. D. Carlos, H. I. S. Nogueira, *Cryst. Growth Des.*, 2008, **8**, 2505–2516; (e) N. Kerbellec, D. Kustaryono, V. Haquin, M. Etienne, C. Daiguebonne, O. Guillou, *J. Inorg. Chem.*, 2009, **48**, 2837–2843; (f) E. Chelebaeva, J. Long, J. Larionova, R. A. S. Ferreira, L. D. Carlos, F. A. Almeida Paz, J. B. R. Gomes, A. Trifonov, C. Guérin, Y. Guari, *Inorg. Chem.*, 2012, **51**, 9005–9016; (g) D. T. de Lill, A. de Bettencourt-Dias, C. L. Cahill, *Inorg. Chem.*, 2007, **46**, 3960–3965; (h) I. G. Fomina, Zh. V. Dobrokhotova, G. G. Aleksandrov, V. I. Zhilov, I. P. Malkerova, A. S. Alikhanyan, D. M. Zhigunov, A. S. Bogomyakov, V. I. Gerasimova, V. M. Novotortsev, I. L. Eremenko, *Polyhedron*, 2013, **50**, 297–305.
- 5 (a) I. G. Fomina, M. A. Kiskin, A. G. Martynov, G. G. Aleksandrov, Zh. V. Dobrokhotova, Yu. G. Gorbunova, Yu. G. Shvedenkov, A. Yu. Tsivadze, V. M. Novotortsev, I. L. Eremenko, *Russ. J. Inorg. Chem.*, 2004, **49**, 1349–1359; (b) I. G. Fomina, Zh. V. Dobrokhotova, V. O. Kazak, G. G. Aleksandrov, K. A. Lysenko, L. N. Puntus, V. I. Gerasimova, A. S. Bogomyakov, V. M. Novotortsev, I. L. Eremenko, *Eur. J. Inorg. Chem.*, 2012, **22**, 3595–3610; (c) Zh. V. Dobrokhotova, I. G. Fomina, G. G. Aleksandrov, Yu. A. Velikodnyi, V. N. Ikorskii, A. S. Bogomyakov, L. N. Puntus, V. M. Novotortsev, I. L. Eremenko, *Russ. J. Inorg. Chem.*, 2009, **54**, 668–685; (d) I. G. Fomina, Zh. V. Dobrokhotova, A. B. Ilyukhin, G. G.

- Aleksandrov, V. O. Kazak, A. E. Gehman, N. N. Efimov, A. S. Bogomyakov, Y. S. Zavorotny, V. I. Gerasimova, V. M. Novotortsev, I. L. Eremenko, *Polyhedron*, 2013, **65**, 152–160.
- 6 *SMART (Control) and SAINT (Integration) Software*, Version 5.0, Bruker AXS Inc., Madison, WI, 1997.
- 7 G. M. Sheldrick, *SADABS, Program for Scanning and Correction of Area Detector Data*, Göttingen University, Göttingen, Germany, 2004.
- 8 G. M. Sheldrick, *Acta. Crystallogr.*, 2008, **A64**, 112–122.
- 9 W. V. Ligon, *Anal. Chem.*, 1978, **50**, 1228-1229.
- 10 I. G. Fomina, Zh. V. Dobrokhotova, A. B. Ilyukhin, G. G. Aleksandrov, A. V. Gavrikov, A. S. Bogomyakov, A. E. Gehman, Y. S. Zavorotny, V. I. Gerasimova, V. M. Novotortsev, I. L. Eremenko, *Russ. Chem. Bull.* **2014**, *63*, 938-944.
- 11 X. Li, Y.-L. Ju, Y-Q. Li, *Coord. Chem.*, 2008, **61**, 692-704.
- 12 S. P. Wang, L. J. Xu, Z. H. Gao, R. F. Wang, *Russ. J. Coord. Chem.*, 2010, **36**, 786-792.
- 13 <http://webbook.nist.gov>.
- 14 (a) O. Carp, L. Patron, I. Mindru, G. Marinescu, L. Diamandescu, A. Banuta, *J. Therm. Anal. Calorim.*, 2003, **74**, 789-799; (b) M. Hamid, A. A. Tahir, M. Mazhar, M. Zeller, K. C. Molloy, A. D. Hunter, *Inorg. Chem.* 2006, **45**, 10457-10466; (c) K. O. Abdulwahab, M. A. Malik, P. O'Brien, G. A. Timco, F. Tuna, C. A. Muryn, R. E. P. Winpenny, R. A. D. Patrick, V. S. Coker, E. Arenholz, *Chem. Mater.*, 2014, **26**, 999–1013; (d) Zh. Dobrokhotova, A. Emelina, A. Sidorov, G. Aleksandrov, M. Kiskin, P. Koroteev, M. Bykov, M. Fazylybekov, A. Bogomyakov, V. Novotortsev, I. Eremenko, *Polyhedron*, 2011, **30**, 132-141; (e) Q. Tang, S-X. Liu, D.-D. Liang, F.-J. Ma, G.-J. Ren, F. Wei, Y. Yang, C.-C. Li, *Solid State Chem.*, 2012, **190**, 85–91.
- 15 (a) J.-M. Rueff, N. Barrier, S. Boudin, V. Dorcet, V. Caignaert, P. Boullay, G. B. Hix, P.-A. Jaffr, *Dalton Trans.*, 2009, **38**, 10614-10620; (b) F. R. G. de Silva, E. P. Marinho, R. S. de Oliveira, M. A. D. Navarro, D. M. A. Melo, K. Zinner, L. B. Zinner, G. J. Vicentini, *Alloys Compd.*, 2004, **374**, 354-357; (c) Y.-G. Huang, F.-L. Jiang, D.-Q. Yuan, M.-Y. Wu, Q. Gao, W. Wei, M.-C. Hong, *Solid State Chem.*, 2009, **182**, 215-222; (d) I. G. Fomina, Zh. V. Dobrokhotova, G. G. Aleksandrov, A. L. Emelina, M. A. Bykov, I. P. Malkerova, A. S. Bogomyakov, L. N. Puntus, V. M. Novotortsev, I. L. Eremenko, *J. Solid State Chem.*, 2012, **185**, 49–55.

- 16 Y. Song, F. Luo, M. Luo, Z. Liao, G. Sun, X. Tian, Y. Zhu, Z. Yuan, S. Liu, W. Xu, X. Feng, *Chem. Commun.*, 2012, **48**, 1006–1008.
- 17 I. P. Malkerova, A. S. Alikhanyan, I. G. Fomina, Zh. V. Dobrokhotova, *Russ. J. Inorg. Chem.* 2009, **54**, 734-737.
- 18 I. P. Malkerova, A. S. Alikhanyan, I. G. Fomina, Zh. V. Dobrokhotova, *Russ. J. Inorg. Chem.*, 2010, **55**, 53-57.
- 19 M. Latva, H. Takalo, V.-M. Mikkala, C. Matachescu, J.-C. Rodrigues-Ubis, J. Kankare, *J. Lumin.*, 1997, **75**, 149-169.
- 20 C.-L. Choi, Y.-F. Yen, H. H.-Y. Sung, A. W.-H. Siu, S. T. Jayarathne, K. S. Wong, I. D. Williams, *J. Mater. Chem.*, 2011, **21**, 8547-8549.
- 21 Z.-G. Yan, Y.-W. Zhang, L.-P. You, R. Si, C. H. Yan, *Sol. State Comm.*, 2004, **130**, 125-129.
- 22 Y. Luo, G. Calvez, S. Freslon, K. Bernot, C. Daiguebonne, O. Guillou, *Eur. J. Inorg. Chem.*, 2011, 3705-3716.
- 23 V. L. Levshin, *Photoluminescence of Liquids and Solids*, Gos. Izd. Tekhniko-teoreticheskoi literatury, Moscow, Leningrad, 1951, p. 96 (in Russian).
- 24 W. T. Carnall, H. Crosswhite, H. M. Crosswhite, *Energy level structure and transition probabilities in the spectra of the trivalent lanthanides in LaF<sub>3</sub>*, Argonne National Laboratory, 1977, Internal Report.
- 25 (a) I. M. Alaoui, *J. Phys. Chem.*, 1995, **99**, 13280-13282; (b) G.-L. Law, W.-M. Kwok, W.-T. Wong, K.-L. Wong, P. A. Tanner, *J. Phys. Chem. B*, 2007, **111**, 10858-10861.

As the temperature decreases to 77 K, the PL decay time of  $\text{Tb}^{3+}$  ions in  $[\text{SmTb}(\text{piv})_6(\text{phen})_2]$  and  $[\text{SmTb}(\text{piv})_6(\text{bath})_2] \cdot 1.75\text{EtOH}$  increase to 1.3 ms, which accompanied by a evidently change of PL color of compounds to bright green, comparing to red at 300 K. This is due to a decrease in the efficiency of nonradiative excited state relaxation channel from the  $^5\text{D}_4$  level of  $\text{Tb}^{3+}$  ions.

